

# **The Investigation of Glutamine and Glutamate in the Human Brain Using MR Spectroscopy at 7 Tesla**

**Dissertation**

zur Erlangung des akademischen Grades

**doctor rerum naturalium**

**(Dr. rer. nat.)**

genehmigt durch die Fakultät für Naturwissenschaften  
der Otto-von-Guericke-Universität Magdeburg

von **M.Sc. Weiqiang Dou**

geb. am 25.05.1985 in Nanjing, People's Republic of China

Gutachter: **Prof. Dr. rer. nat. Oliver Speck**

Gutachter: **Prof. Dr. rer. nat. Uwe Klose**

eingereicht am: 10.06.2014

verteidigt am: 27.10.2014

*To my parents and my wife (Sally Pingping)*

## Table of Contents

---

# Table of Contents

ABSTRACT.....	i
ZUSAMMENFASSUNG .....	iii
LIST of ABBREVIATION .....	v
Introduction .....	1
1.1 Motivation.....	2
1.2 Outline of the Thesis.....	4
Foundations .....	6
2.1 Nuclear Magnetic Resonance .....	7
2.1.1 Background .....	7
2.1.2 Chemical Shift .....	7
2.1.3 J-Coupling Effect .....	9
2.1.4 Multiplicity .....	10
2.2 In Vivo Single Voxel Proton Magnetic Resonance Spectroscopy ( <sup>1</sup> H-MRS).....	10
2.2.1 Background .....	10
2.2.2 Techniques for Spatial Localization .....	11
2.2.3 Spectral Analysis .....	14
Comparing Gln/Glu Separation Using STEAM with Short and Long TE/TM at 3 and 7 T .	19
3.1 Preface .....	20
3.2 Background .....	22
3.2.1 Glutamate and Glutamine.....	22
3.2.2 Effect of TE/TM on Gln and Glu .....	24
3.3 Materials and Methods.....	30
3.3.1 Spectral Simulation for Gln and Glu.....	30
3.3.2 Phantom Results .....	30
3.3.3 <i>In Vivo</i> Results .....	31
3.3.4 Basis Set Making .....	33
3.3.5 Data Analysis.....	34
3.4 Results.....	35
3.4.1 Simulation Results.....	35
3.4.2 Phantom Results .....	36
3.4.3 <i>In Vivo</i> Results.....	38
3.5 Discussion.....	41
Measurement Reproducibility and Systematical Investigations of GABA, Gln and Glu Concentrations Using STEAM with Short TE/TM at 7 T .....	45
4.1 Preface .....	46
4.2 Materials and Methods.....	47
4.3 Results.....	51
4.3.1 Spectrum Quality .....	51
4.3.2 Regional Variations of Gray Matter across Human Cingulate Cortex .....	52
4.3.3 The Reproducibility of Repeated Measurements.....	53
4.3.4 The Regional Variations of GABA, Gln and Glu Concentrations and Ratios in the Cingulate Cortex .....	54

# Table of Contents

---

4.3.5	The Effects of the Voxel Placement Deviations on Metabolite Concentrations.....	57
4.4	Discussion.....	58
	Automatic Voxel Positioning for MR Spectroscopy at 7 T .....	62
5.1	Preface .....	63
5.2	Materials and Methods.....	64
5.3	Results.....	68
5.4	Discussion.....	72
	Summary .....	75
	BIBLIOGRAPHY .....	79
	OWN PUBLICATIONS.....	88
	ACKNOWLEDGEMENTS.....	90
	ERKLÄRUNG .....	91
	LEBENS LAUF .....	92

# ABSTRACT

The concentrations of the primary excitatory neurotransmitter glutamate (Glu) and its precursor glutamine (Gln) are directly linked to a variety of neurological and psychiatric disorders. However, accurate non-invasive *in vivo* detection of both metabolites through magnetic resonance spectroscopy (MRS) is limited by their very similar chemical shifts and J-coupling constants, resulting in severely overlapping multiplet signals that are difficult to separate.

Stimulated echo acquisition mode (STEAM), as an advanced proton MRS ( $^1\text{H}$ -MRS) method, has been proven to detect metabolites simultaneously and efficiently. Yang et al., (2008) proposed field-specific long echo time (TE) / mixing time (TM) settings for 3 to 9.4 T to optimally separate the main peaks of Gln and Glu in STEAM acquisitions. In the meanwhile, short TE STEAM was also suggested to measure *in vivo* Gln and Glu at high field strengths, since short TE provides high spectral signal-to-noise-ratio (SNR) and the enhanced chemical shift dispersion at strong field strengths can partially resolve the spectral overlap between Gln and Glu.

Due to the above-mentioned different advantages for Gln and Glu acquisitions at short and long TE/TM, the first goal of this study was to determine the best TE/TM setting for Gln and Glu acquisitions at 7 T by systematically investigating the Gln and Glu signals at short TE/TM and 7 T-specific long TE/TM in simulations, in *in vitro* and *in vivo* experiments. The results demonstrated that the application of short TE/TM in STEAM can provide more accurate *in vivo* Gln and Glu detection at 7 T.

Applying STEAM with short TE/TM, local Gln and Glu signals across human cingulate cortex (CC) were systematically measured and quantified. The measurement reproducibility for Gln and Glu, as the second goal of this thesis, was quantified and confirmed. Additionally, the regional variations of local Gln and Glu concentrations

## ABSTRACT

---

across CC were revealed and compared to the density distributions of local receptors for the first time.

The last goal of this thesis was to test for the first time whether MRS voxels can be prescribed automatically with sufficient reliability in a high field longitudinal MRS study. Using a vendor-provided automatic voxel positioning technique developed for lower field strength, highly reliable automatic MRS voxel prescription was achieved. Automatic voxel prescription with higher accuracy and reproducibility, compared to manual voxel prescription, is thus suggested to be applied in future high field longitudinal MRS studies.

# ZUSAMMENFASSUNG

Die Konzentrationen der wichtigsten exzitatorischen Neurotransmitter Glutamat (Glu) und seiner Vorstufe Glutamin (Gln) sind direkt mit einer Vielzahl von neurologischen und psychiatrischen Störungen verbunden. Ein genauer nicht-invasiver Nachweis beider Metaboliten *in vivo* mittels Magnetresonanztomographie (MRS) wird jedoch durch ihre sehr ähnlichen chemischen Verschiebungen und J-Kopplungskonstanten sowie durch stark überlappende und schwer trennbare Multiplettsignale begrenzt.

Stimulated echo acquisition mode (STEAM) ist eine etablierte Methode der Protonen-MRS ( $^1\text{H}$ -MRS) zur gleichzeitigen und effizienten Messung von Metaboliten. Yang et al., (2008) schlugen feldspezifisch lange Echozeiten (TE) und Mischzeiten (TM) für 3 – 9.4 T vor, um die wichtigsten Signale von Gln und Glu mit STEAM optimal zu trennen. Dagegen wurde auch eine kurze TE für STEAM vorgeschlagen, um Gln und Glu *in vivo* bei hohen Feldstärken zu messen, da eine kurze TE ein hohes spektrales Signal-Rausch-Verhältnis (SNR) ermöglicht. Durch die erhöhte Dispersion der chemischen Verschiebung bei hohen Feldstärken kann die spektrale Überlappung zwischen Gln und Glu teilweise aufgelöst werden.

Aufgrund der oben genannten Vorteile für die Detektion von Gln und Glu bei kurzen und langen TE/TM war das erste Ziel dieser Studie, die besten TE/TM-Einstellungen zur Detektion von Gln und Glu bei 7 T zu bestimmen. Es wurden Gln und Glu Signale bei kurzen TE/TM und langen TE/TM in Simulationen sowie in *in vitro* und *in vivo* Experimenten systematisch untersucht. Die Ergebnisse zeigen, dass die Anwendung von kurzen TE/TM mit STEAM eine genauere *in vivo* Detektion von Gln und Glu bei 7 T erlaubt.

Unter Anwendung von STEAM mit kurzen TE/TM wurden Einzelvoxel-Spektren im cingulären Cortex (CC) bei Probanden systematisch aufgenommen sowie Gln und Glu

## ZUSAMMENFASSUNG

---

Konzentrationen quantifiziert. Als zweites Ziel dieser Arbeit wurde die Reproduzierbarkeit der Quantifizierung für Gln und Glu bestätigt. Zusätzlich wurden regionale Unterschiede der lokalen Gln und Glu Konzentrationen über den gesamten CC zum ersten Mal gezeigt und mit den Dichteverteilungen lokaler Rezeptoren verglichen.

Das letzte Ziel dieser Arbeit war es, erstmals im Zeitverlauf bei hoher Feldstärke zu testen, ob MRS-Voxel mit ausreichender Zuverlässigkeit automatisch repositioniert werden können. Mit einer vom Hersteller bereitgestellten automatischen Voxel-Repositionierungstechnik, die für geringere Feldstärken entwickelt wurde, wurden äußerst zuverlässige automatische MRS-Voxel-Repositionierungen erreicht. Für zukünftige MRS-Zeitverlaufsstudien empfiehlt sich daher die automatische Voxel-Repositionierung mit höherer Genauigkeit und Reproduzierbarkeit im Vergleich zur manuellen Voxel-Repositionierung.

## LIST of ABBREVIATION

---

# LIST of ABBREVIATION

<b>Meaning</b>	<b>Abbreviation</b>
Absolute Concentration	Abs. Con.
Analysis of Variance	ANOVA
Anterior Cingulate Cortex	ACC
Anterior Commissure	AC
Anterior Mid-Cingulate Cortex	aMCC
Bandwidth	BW
Carbon-4	C4
Caudal Posterior Cingulate Cortex	cPCC
Cerebrospinal Fluid	CSF
Choline	Cho
Cingulate Cortex	CC
Correlation Coefficient	Corr. Coef.
Cramer-Rao Lower Bound	CRLB
Default Mode Network	DMN
Echo Time	TE
Flip Angle	FA
Full Width At Half Maximum	FWHM
Functional Magnetic Resonance Imaging	fMRI
Glutamate	Glu
Glutamine	Gln
Glutamate + Glutamine	Glx
Gray Matter	GM
Institutional Units	i.u.
Intraclass Correlation Coefficient	ICC
Inversion Time	TI

## LIST of ABBREVIATION

---

Magnetic Resonance	MR
Magnetic Resonance Spectroscopy	MRS
Magnetization-Prepared Rapid Gradient Echo	MPRAGE
Mid-Cingulate Cortex	MCC
Mixing Time	TM
N-acetylaspartate	NAA
Nuclear Magnetic Resonance	NMR
Parts Per Million	ppm
Point Resolved Spectroscopy	PRESS
Posterior Cingulate Cortex	PCC
Posterior Commissure	PC
Pregenual Anterior Cingulate Cortex	pgACC
Proton Magnetic Resonance Spectroscopy	<sup>1</sup> H-MRS
Radio Frequency	RF
Regions Of Interest	ROIs
Repetition Time	TR
Rostral Posterior Cingulate Cortex	rPCC
Signal-To-Noise-Ratio	SNR
Standard Deviation	SD
Stimulated Echo Acquisition Mode	STEAM
Three Dimensional	3D
Variable Rate Selective Excitation	VERSE
Versatile Simulation, Pulses and Analysis for Magnetic Resonance Spectroscopy	VeSPA
White Matter	WM

*1*

# **Introduction**

### 1.1 Motivation

Magnetic resonance spectroscopy (MRS), as a non-invasive technique measuring metabolites *in vivo*, has rapidly developed in the past several decades. Using gradients, MRS technique is able to selectively excite regions of interest and measure neuro-metabolites in specific regions with small volumes by observing the signals of a specific nucleus (e.g.,  $^1\text{H}$ ,  $^{13}\text{C}$  and  $^{31}\text{P}$ ; Mandal, 2007).

$^1\text{H}$ -MRS is one of the most widely applied techniques in basic or clinical studies, since the proton  $^1\text{H}$ , the most abundant nuclear isotope (99.8%; Blümich, 2005, 16), can provide higher sensitivity compared to other nuclei. With increased magnetic field strengths, accurate metabolite detection using  $^1\text{H}$ -MRS becomes less challenging, e.g., for metabolites with singlet like N-acetylaspartate, creatine and choline at the field strengths of 1.5 T and 3 T (Bartha et al., 2000; Frahm et al., 1989; Kreis et al., 1993). However, the acquisitions for metabolites with multiplets, especially for those having close chemical shifts and thus difficulties for separation, e.g., glutamine (Gln) and glutamate (Glu), are usually technically limited at field strengths up to 4.7 T (Yang et al., 2008), so that the measured Gln and Glu are in many cases combined and only expressed as Glx (Gln + Glu).

Glutamate, as the primary excitatory neurotransmitter in the central nervous system (Erecinska and Silver, 1990), is rapidly taken up into astrocytes and synthesized into Gln. Glutamine then crosses the membranes of glial cells to be transported into nerve cell terminals and converted into Glu again (Levine et al., 2000). The abnormal levels of Gln, Glu or the ratio of Gln/Glu cycling were reported to directly link to a variety of neurological and psychiatric disorders including epilepsy, major depression disorder, uni- and bi-polar disorders (Petroff et al., 1996; Sanacora et al., 1999; Yildiz-Yesiloglu et al., 2006; Altamura et al., 1995; Brambilla et al., 2005). Therefore, reliable acquisitions of Gln and Glu in parallel, as well as the corresponding accurate quantification of the two, are highly desired in clinical studies and thus must be accomplished.

## Introduction

---

To date, a number of  $^1\text{H}$ -MRS techniques have been applied for effective detections of Gln and Glu at 1.5 T and 3 T. They include: 1) point resolved spectroscopy (PRESS) with constant echo time (TE; Schubert et al., 2004; Mayer and Spielman, 2005); 2) spectral editing techniques, e.g., the multiple quantum coherence filtering (Thompson and Allen, 1998) and J-refocused editing and coherence transfer (Lee et al., 1995; Pan et al., 1996); 3) 2D spectroscopy, such as TE-averaged PRESS (Hurd et al., 2004), 2D J-resolved spectroscopy (Thomas et al., 1996) and the chemical shift selective filter (Schulte et al., 2005). However, the PRESS technique with constant TE, i.e., 80 ms, can only optimally detect Glu but not Gln. The spectral editing techniques are not capable of focusing on Gln and Glu simultaneously but losing either Gln or Glu during spectrum acquisitions. 2D spectroscopy are usually time consuming (16 – 30 ms) for one region measurement and require large voxel size (16 - 27 ml). In clinical MRS, the slow rate of acquisition is a challenge for patients, and the required large voxel size can produce strong partial volume effects and prevent the investigations of small yet highly specific brain regions.

Due to increased chemical shift dispersion and spectral sensitivity in high field MR scanner, e.g., 7 T, the spectra of Gln and Glu become feasible to be well resolved (Tkáč et al., 2001; Stephenson et al., 2011; Elywa et al., 2012). As an advanced single voxel  $^1\text{H}$ -MRS technique, stimulated echo acquisition mode (STEAM) is, in principle, able to detect *in vivo* metabolites simultaneously within small MRS voxels and allow for rapid spectrum acquisitions (Graaf and Rothman, 2001). Basing on both advantages, STEAM is considered being potentially suitable for clinical MRS studies. One novel study Yang et al., (2008) simulated the spectral responses of Gln and Glu in STEAM acquisitions with a range of TEs and mixing times (TMs) for 3 T to 9.4 T. This study proposed field-specific long TE/TM settings to optimally resolve Gln and Glu signals of the Carbon-4 (C4) proton resonances which are the main peaks of Gln and Glu spectra. In the mean while, short TE STEAM was also suggested previously to be applied at high field 7 T for *in vivo* Gln and Glu acquisitions, since short TE for high spectral signal-to-noise-ratio (SNR) together with the above-mentioned high chemical shift dispersion at 7 T for partially resolving

# Introduction

---

spectral overlap can provide reliable acquisitions of Gln and Glu and thus low Cramer-Rao lower bound (CRLB) values of Gln and Glu (Tkáč et al., 2001; Stephan et al., 2011). Although both short and field-specific long TE/TM have respective advantages for Gln and Glu detection, it remains however unclear whether the optimal spectral separation between Gln and Glu and thus the accurate metabolite quantification can be achieved by 7 T-specific long TE/TM or the higher spectral SNR at short TE/TM. Therefore, the first goal in this thesis is to determine the optimal TE/TM setting in STEAM for *in vivo* Gln and Glu acquisitions and separation at 7 T.

Using STEAM with the determined optimal TE/TM setting, local Gln and Glu signals across human cingulate cortex (CC) are to be systematically measured at 7 T. The reproducibility of Gln and Glu measurements, as the second goal of this thesis, is going to be quantified and assessed. In addition, the regional variations of local Gln and Glu as well as GABA in the cingulate sub-regions will be revealed for the first time.

In longitudinal clinical MRS studies, manual voxel prescription as the traditional method for voxel placement can in many cases introduce the variability of voxel positions between different scan sessions and require extra scan time for voxel adjustments (e.g., voxel localizations and orientations; Itti et al., 2001; Benner et al., 2006). Due to the potential interference between high field image intensity variations and voxel position detection, no automatic voxel positioning technique has been applied so far in high field MRS studies. Therefore, the third goal of this thesis is to test whether automatic voxel prescription can be achieved with high accuracy and reproducibility in a 7 T longitudinal *in vivo* MRS study.

## 1.2 Outline of the Thesis

In Chapter 2, the basic knowledge regarding nuclear magnetic resonance (NMR) spectroscopy is firstly introduced, including the background of NMR, chemical shift, J-

## Introduction

---

coupling effect and so on. Secondly, the single voxel  $^1\text{H}$ -MRS and its two most widely used techniques, namely, PRESS and STEAM, are presented. Lastly, a routine pipeline for spectrum analysis using LCModel is listed and explained.

In Chapter 3, STEAM spectra of Gln and Glu at short and field-specific long TE/TM are acquired in simulations, and the corresponding *in vitro* and *in vivo* Gln and Glu signals are measured at 3 and 7 T. These field-specific Gln and Glu signals are analyzed and compared to determine the optimal TE/TM setting for Gln and Glu acquisitions and separation.

In Chapter 4, STEAM with the optimal TE and TM determined in Chapter 3 is applied at 7 T to systematically measure the local signals of Gln and Glu in four sub-regions across human CC. The reproducibility of Gln and Glu acquisitions are estimated, and the concentration distributions of local Gln, Glu and GABA across the CC are revealed for the first time.

In Chapter 5, a vendor-provided automatic voxel positioning technique is applied for the first time to prescribe spectroscopy voxels in a 7 T longitudinal *in vivo* MRS study. The accuracy and reproducibility of automatic voxel prescription are assessed and further compared to manual voxel prescription.

Lastly, in Chapter 6, the above mentioned works are discussed and summarized.

All the works mentioned in Chapter 3, 4 and 5 were performed at Otto-von-Guericke-University Magdeburg and supported by DFG (Wa2673/3-1).

# 2

## Foundations

## 2.1 Nuclear Magnetic Resonance

### 2.1.1 Background

Nuclear Magnetic Resonance (NMR) is a physical phenomenon used to investigate molecular properties of matter irradiating atomic nuclei in a magnetic field with radio waves (Blümich, 2005, 2; Jacobsen, 2007, 1). Based on the magnetic resonance for certain nucleus, NMR is a spectroscopic technique of determining the chemical structure of the unknown compounds and is also a powerful tool for observing the dynamic processes that may occur within or between molecules, e.g., bond rotation about bond axes, ring inversion, tautomerism (intra- and inter-molecular exchange of nuclei between functional groups) and etc. (Balcli, 2005, 213). The nuclei of  $^1\text{H}$ ,  $^{13}\text{C}$ ,  $^{15}\text{N}$  and  $^{31}\text{P}$  are the most commonly used in NMR spectroscopy (Blümich, 2005, 16; Jacobsen, 2007, 1). In this chapter, the NMR with the proton  $^1\text{H}$  is taken as an example to explain the concepts of chemical shift, J-coupling effect and multiplicity.

### 2.1.2 Chemical Shift

The Larmor frequency  $\nu_0$  of a free single proton spin is given by the Larmor equation (Becker, 2000, 88):

$$\nu_0 = \gamma \cdot B_0 \quad [\text{Eq.2.1}]$$

, where  $\gamma$  is the gyromagnetic ratio (42.6 MHz/T for  $^1\text{H}$ ) and  $B_0$  is the field strength of the external static magnetic field.

In atoms and molecules, a proton  $i$  is shielded by electrons. It does not experience the static field  $B_0$  but a magnetic field  $B_i$ , arising from superposition of the  $B_0$  field and an additional field  $B_{ind,i}$  induced by the shielding electrons (Keeler, 2002, 2-2; Breitmaier and Voelter, 1987, 15) :

## Foundations

---

$$\mathbf{B}_i = \mathbf{B}_0 - \mathbf{B}_{ind,i} \quad [\text{Eq.2.2}]$$

The strength of  $B_{ind,i}$  induced by the electrons is proportional to the strength of the applied  $B_0$ :

$$\mathbf{B}_{ind,i} = \sigma_i \cdot \mathbf{B}_0 \quad [\text{Eq.2.3}]$$

, where the factor  $\sigma_i$  is called the magnetic shielding constant for the proton  $i$ , and characterizes the chemical environment of that proton.

According to the above mentioned Eq.2.2 and Eq.2.3, the effective field  $B_i$  experienced by the proton  $i$  is calculated:

$$\mathbf{B}_i = \mathbf{B}_0 \cdot (1 - \sigma_i) \quad [\text{Eq.2.4}]$$

Thus, the proton  $i$  precesses at the Larmor frequency  $V_{0,i}$  when exposed to the static magnetic field  $B_0$ :

$$V_{0,i} = \gamma \cdot \mathbf{B}_0 \cdot (1 - \sigma_i) \quad [\text{Eq.2.5}]$$

Therefore, the shift of Larmor frequencies due to the chemical nonequivalence of protons in molecules is called the chemical shift (Breitmaier and Voelter, 1987, 15).

Chemical shifts are measured with reference to the absorption signal of a reference compound appearing at frequency  $V_{ref}$  (Hz). The most commonly used reference compound is tetramethylsilane (TMS; Balcli, 2005, 29).

If the proton  $i$  has the frequency  $V_i$  (Hz) and the frequency of the TMS is  $V_{TMS}$  (also in Hz), the chemical shift  $\delta$  of nucleus is computed as (Keeler, 2002, 2-2):

$$\delta = \frac{V_i - V_{TMS}}{V_{TMS}} \quad [\text{Eq.2.6}]$$

## Foundations

---

Typically, the chemical shift  $\delta$  is rather small, so it is common to multiply the value by  $10^6$  and then quote its value in *parts per million* (ppm):

$$\delta(\text{ppm}) = 10^6 \cdot \frac{V_i - V_{TMS}}{V_{TMS}} \quad [\text{Eq.2.7}]$$

With this definition, the chemical shift of the reference compound is 0 ppm.

### 2.1.3 J-Coupling Effect

In addition to the chemical shift, there is another molecular interaction that modifies the environment of a proton. Protons located on the same molecule interact with each other and each has its local magnetic field affected. The most common instance of this in biological systems is facilitated by the bonding electrons in the molecule and is known as J-coupling. Unlike chemical shift, J-coupling is independent of magnetic field strength and there is always another spin involved in the coupling (Brown and Semelka, 2003, 182).

J-coupling is the only factor that determines the splitting patterns of the signals (Balci, 2005, 139). In the proton NMR spectrum, each signal is split into a multiple peak pattern by the influence of its “neighbors”, the proton attached to the next carbon in the chain. Consider two protons ( $^1\text{H}_a\text{C}-\text{C}^1\text{H}_b$ ) with different chemical shifts on two adjacent carbon atoms in a molecule. The magnetic nucleus of  $H_b$  can be either aligned with (“up”) or against (“down”) the magnetic field. From the point of view of  $H_a$ , the  $H_b$  nucleus magnetic field perturbs the external magnetic field, adding a slight amount to it or subtracting a slight amount from it, depending on the orientation of the  $H_b$  nucleus (“up” or “down”). Because the resonant frequency is proportional to the magnetic field experienced by the nucleus due to Eq.2.1, this changes the  $H_a$  frequency so that it now resonates at both frequencies. Because roughly 50% of the  $H_b$  nuclei are in the “up” state and roughly 50% are in the “down” state, the  $H_a$  resonance is split by  $H_b$  into a pair

## Foundations

---

of resonance peaks of equal intensity (a “doublet”) with a separation of J Hz, where J is called the J coupling constant. The relationship is mutual so that  $H_b$  experiences the same splitting effect (separation of J Hz) from  $H_a$  (Jacobsen, 2007, 4).

There are two different kinds of J-coupling spin systems: weakly coupled spin systems and strong coupled spin system. Weakly coupled spin system is defined as when the Larmor frequencies of spins are much greater in magnitude than the magnitude of the couplings between spins, whereas strongly coupled spin system is the spin system in which the separation of the Larmor frequencies of spins are much lower than the coupling constants (Keeler, 2002, 2-14).

### 2.1.4 Multiplicity

Multiplicity of the split is determined by the number of protons. The signal of a proton that has  $n$  equivalent neighboring protons is split into a multiplet of  $n+1$  peaks (Balci, 2005, 96-97).

## 2.2 *In Vivo* Single Voxel Proton Magnetic Resonance Spectroscopy ( $^1\text{H}$ -MRS)

### 2.2.1 Background

The fundamental basis of magnetic resonance spectroscopy (MRS) is governed by the same principles of NMR introduced in the previous section (Mandal, 2007). As the most abundant nuclear isotope (99.8%) in nature, the proton  $^1\text{H}$  is one of the most observed nuclei using MRS technique (Graaf and Rothman, 2001). In numerous studies, proton MRS ( $^1\text{H}$ -MRS) has been applied to measure metabolites *in vivo* (Graaf and Rothman, 2001).

## 2.2.2 Techniques for Spatial Localization

$^1\text{H}$ -MRS has demonstrated that it is possible to obtain high resolution spectra from small well-defined regions (Mandal, 2007). These regions are selected using three-dimension oriented radio frequency (RF) pulses when spatial localization techniques are applied (Fig. 2.1). Generally, spatial localization techniques contain single voxel and multiple voxel techniques. Single voxel techniques (also called single voxel spectroscopy) acquire spectra from a single small volume of tissue, whereas multiple voxel techniques localize multiple voxels and acquire the corresponding spectra during a single measurement (Brown and Semelka, 2003, 186-189). As the applied techniques in this thesis, two most frequently used single voxel techniques for  $^1\text{H}$ -MRS are introduced: Point-Resolved Spectroscopy (PRESS) and Stimulated Echo Acquisition Mode (STEAM).

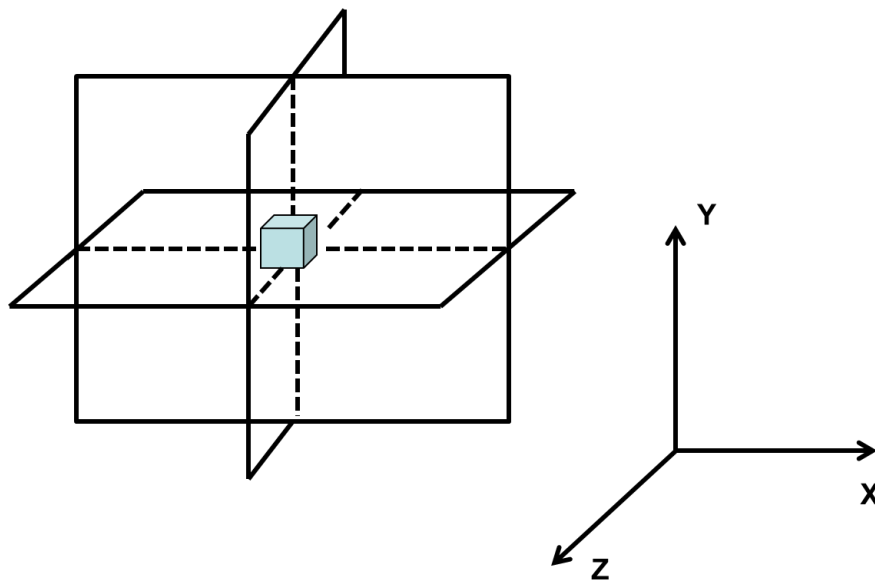


**Figure 2.1** A schematic illustration of selecting a voxel by three orthogonal slice-selecting pulses using spatial localization techniques (Mandal, 2007)

**Point-Resolved Spectroscopy** (Fig. 2.2.A) consists of a  $90^\circ$  excitation pulse and two  $180^\circ$  refocusing pulses. When the first  $180^\circ$  pulse is executed at time  $TE_1/2$  after the excitation pulse, a spin echo is formed at time  $TE_1$ . The second  $180^\circ$  pulse refocuses this spin echo during a delay  $TE_2$ , so that the final spin echo is yielded at time  $TE = TE_1 + TE_2$ .

## Foundations

---

When the three RF pulses are frequency selective and are executed in combination with magnetic field gradients ( $G_x$ ,  $G_y$  and  $G_z$ ), PRESS is capable of three-dimensional localization of a cubic voxel. The first echo at time  $TE_1$  contains signal from a column, which is the intersection between the two orthogonal slices selected by the  $90^\circ$  pulse and the first  $180^\circ$  pulse. The second spin echo only contains signal from the intersection of the three orthogonal planes selected by the three pulses resulting in the desired volume. Signal outside this volume is either not excited or not refocused (Graaf and Rothman, 2001).

**Stimulated Echo Acquisition Mode** (Fig. 2.2.B), similar to PRESS, also uses three mutually orthogonal slice selective pulses and collects only the echo signal from the defined spectroscopy in space where all three slices intersect. The main difference is that STEAM utilizes three slice-selective  $90^\circ$  pulses to achieve localization. As a consequence, STEAM selects a spatially selective stimulated echo, rather than a spin echo as in PRESS.

For both PRESS and STEAM techniques, PRESS is able to provide double the signal from a volume of interest as compared with STEAM, given identical TE. However, STEAM is less sensitive to  $T_2$ -relaxation effects as no  $T_2$ -relaxation occurs during the mixing time (TM), whereas PRESS is sensitive to  $T_2$ -relaxation throughout the localization sequence. In addition, shorter TEs can be achieved using STEAM than using PRESS with the same hardware. Another important factor to consider, especially at high field strengths, is that the amount of transmitter voltage required is approximately two times higher for PRESS than for STEAM, although it is not a significant factor at low fields.

Transmitter voltage, which is proportional to RF power absorbed by subjects, should be taken into account for safety during *in vivo* experiments at high field 7 T. The technique of variable rate selective excitation (VERSE) pulses, which aims to reduce RF power using a time-varying gradient to change the shape of the RF pulse without changing the spatial excitation profile on resonance, was introduced (Hargreaves et al., 2004; Bernstein et al.,

## Foundations

2004, 58-60) and adapted into 7 T STEAM sequence application (Elywa et al., 2012). Fig. 2.3.A shows an example of gradient wave forms with an original constant rate (solid) and a time-varying rate (dash), while Fig. 2.3.B shows the corresponding RF pulse shapes (Conolly et al., 1991). Using the VERSE technique, the amplitude of the RF pulse is reduced by means of stretching its pulse shape when the spatial excitation profile remains the same.

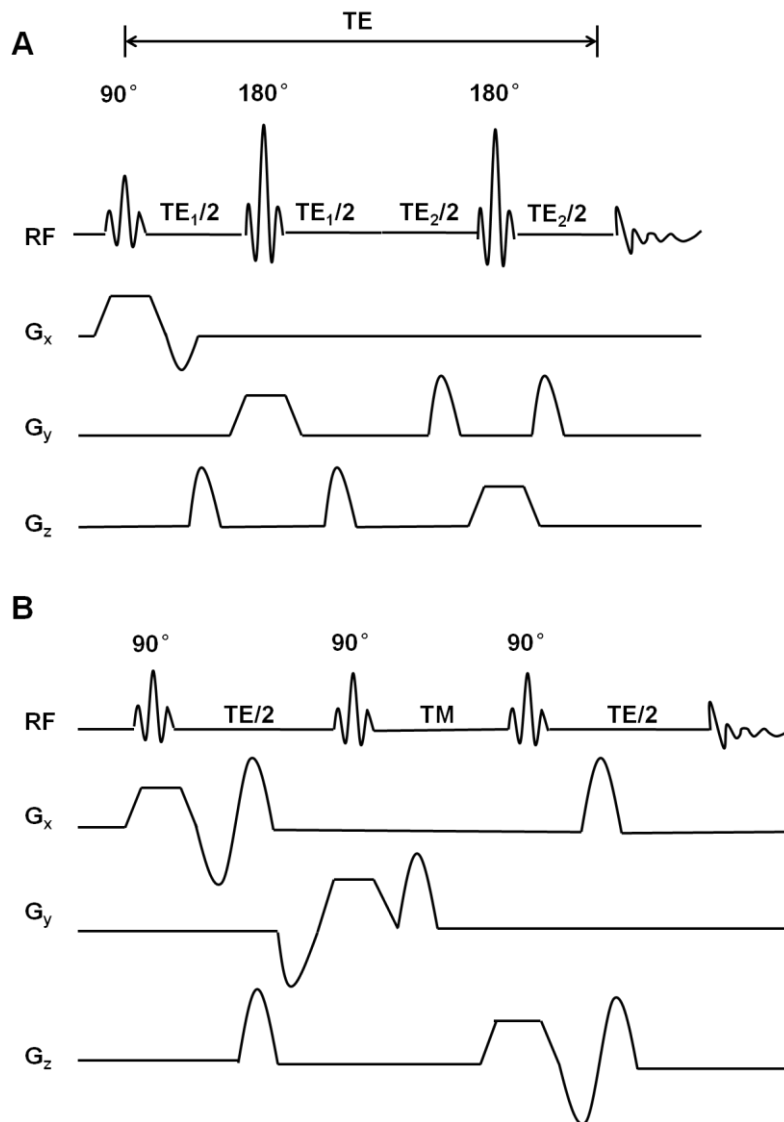


**Figure 2.2** Schematic diagrams of PRESS pulse sequence (A) and STEAM pulse sequence (B) are shown (Graaf and Rothman, 2001).

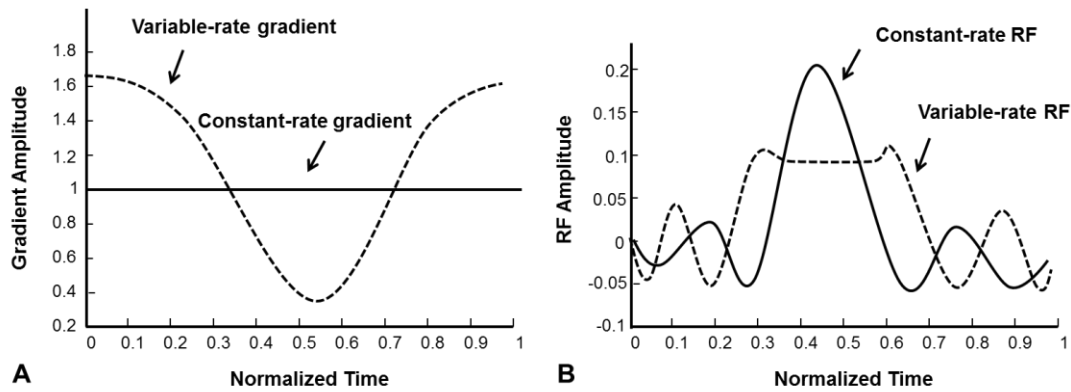


**Figure 2.3** (A) The constant-rate and variable-rate gradient waveforms. (B) The corresponding RF waveforms (Conolly et al., 1991).

## 2.2.3 Spectral Analysis

The MRS signal acquired using PRESS or STEAM technique from the regions of interest contains information regarding the identity, molecular environment, and concentration of the metabolite producing the signal. The information is provided by the resonant frequency, the linewidth, and the integrated peak area, respectively (Brown and Semelka, 2003, 189). Currently, a variety of software is able to analyze MRS signal either in time domain (e.g., MRUI) or frequency domain (e.g., LCModel). Compared to the information extracted from the time domain form (free induction decay signal), it is more convenient to analyze frequency domain form (spectrum) obtained following a Fourier transformation (FT; Brown and Semelka, 2003, 189). The software LCModel is very popular and mostly used in a number of laboratories for spectrum analysis. A corresponding pipeline regarding the spectral analysis using LCModel is described in Fig. 2.4 (Brown and Semelka, 2003, 190).

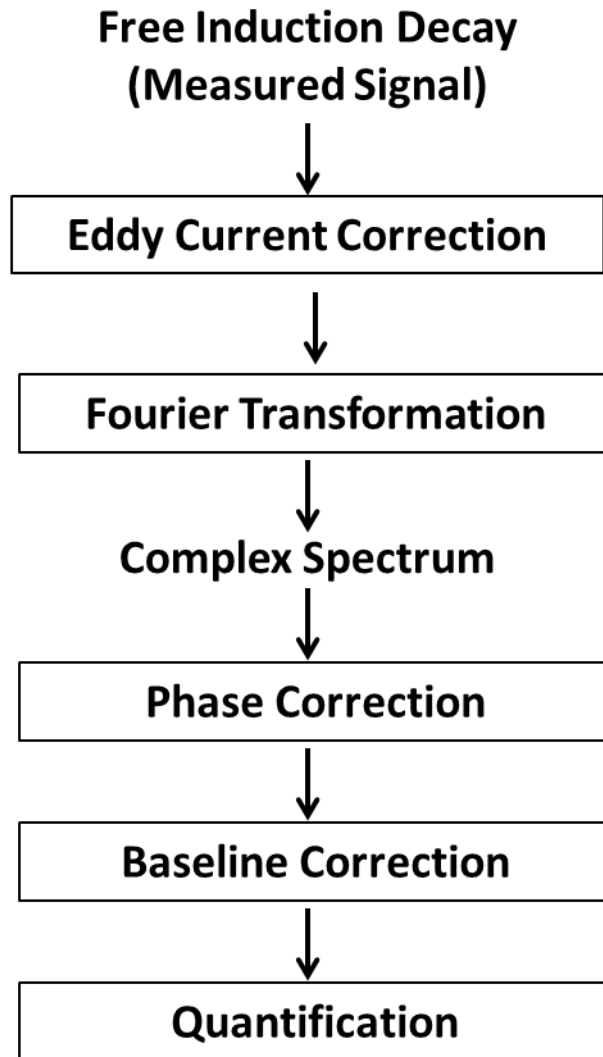


**Figure 2.4** The steps to analyze spectrum using LCModel

### **Eddy Current Correction**

Eddy currents are induced as a result of the time-varying nature of the gradient pulses. They produce time-dependent shifts of the resonance frequency in the selected volume, resulting in a distortion of the spectrum after FT (Brown and Semelka, 2003, 190). To avoid this, a correction method is applied in LCModel that the effect of the eddy currents on the MRS spectrum can be compensated by subtracting the phase of the

## Foundations

---

unsuppressed water signal from the suppressed water signal to be evaluated (Klose, 1990).

### Fourier Transformation

Fourier Transformation is a mathematical algorithm used to convert the free induction decay (FID) signal (measured signal)  $f(t)$  in the time domain into the spectrum  $F(\nu)$  in the frequency domain (Keeler, 2002, 4-2). The conversion is expressed using the following integral:

$$F(\nu) = \int_{-\infty}^{+\infty} f(t) \cdot \exp(-2 \cdot i \cdot \pi \cdot \nu \cdot t) \cdot dt \quad [\text{Eq.2.8}]$$

Supposing the FID signal is:  $f(t) = a \cdot \cos(2 \cdot \pi \cdot \nu' \cdot t) \cdot \exp(-t/T_2^*)$ , the corresponding spectrum  $F(\nu)$  using FT is yielded:

$$\begin{aligned} F(\nu) &= \int_{-\infty}^{+\infty} a \cdot \cos(2 \cdot \pi \cdot \nu' \cdot t) \cdot \exp(-t/T_2^*) \cdot \exp(-2 \cdot i \cdot \pi \cdot \nu \cdot t) \cdot dt \\ &= \int_0^{+\infty} a \cdot \exp(2 \cdot \pi \cdot \nu' \cdot t) \cdot \exp(-t/T_2^*) \cdot \exp(-2 \cdot i \cdot \pi \cdot \nu \cdot t) \cdot dt \\ &= a \cdot \frac{T_2^*}{1 + 4 \cdot \pi^2 \cdot (T_2^*)^2 \cdot (\nu' - \nu)^2} + i \cdot \frac{T_2^* \cdot 2 \cdot \pi \cdot (\nu' - \nu)}{1 + 4 \cdot \pi^2 \cdot (T_2^*)^2 \cdot (\nu' - \nu)^2} \\ &= A \cdot (\nu' - \nu) + i \cdot D \cdot (\nu' - \nu) \end{aligned} \quad [\text{Eq.2.9}]$$

The real part A is the absorption spectrum at frequency  $\nu'$ , and the imaginary part D is the dispersion spectrum. The full width at half maximum (FWHM) of the line depends on the decay rate of the relaxation as:  $FWHM = \frac{1}{\pi \cdot T_2^*}$  for the linewidth at half-height (Blümich, 2005, 38).

# Foundations

---

## Phase Correction

Due to the reasons of measuring instruments, there is an unknown phase shift for the signal. In general, this leads to a situation in which the real part of the spectrum does not show a pure absorption lineshape. Therefore, two kinds of phase errors occur: zero order phase error and first order phase error (Keeler, 2002, 4-6). In LCModel, the corresponding phase correction functions zero order phase correction and first order phase correction are applied iteratively for correcting the spectral phase errors (Provencher, 2013, 89).

## Baseline Correction

The baseline is the average of the noise part of the spectrum. Ideally, it would be a straight, horizontal line representing zero intensity. However, in reality, it can drift, roll and wiggle (Jacobsen, 2007, 132-133). These errors may come from the external perturbations or instrumental imperfections during data acquisition or are caused by mis-set acquisition parameters, e.g., incomplete suppression of the water signal (Bigler, 1997, 200-201). The baseline can be automatically adjusted using spline functions in LCModel (Provencher, 2013, 123). A flat baseline is essential for peak area measures, which is important for metabolite quantification.

## Quantification

The LCModel algorithm models the *in vivo*  $^1\text{H}$  MRS spectrum as a linear combination of *in vitro* MRS spectra obtained from metabolite solutions (basis set; Graaf and Rothman, 2001). Since the basis set is generally not measured under identical situations as the *in vivo* MRS measurements, this difference could lead to different scaling. In LCModel, the *in vivo* spectra could be scaled using water scaling factor ( $f_{scale}$ ) to be consistent with the basis set data. Incidentally,  $f_{scale}$  is defined as the ratio of the normalized signal strength in the basis set to the normalized unsuppressed water signal in *in vivo* data. Further, the metabolite absolute concentrations can be calculated (Provencher, 2013, 111):

## Foundations

---

$$Conc_{met} = Ratio_{area} \cdot \left(\frac{2}{N1H_{met}}\right) \cdot \left(\frac{ATT_{H2O}}{att_{met}}\right) \cdot W_{conc}$$

[Eq.2.10]

Where  $Conc_{met}$  is the metabolite concentration;  $Ratio_{area}$  is the ratio of the metabolite resonance area to the unsuppressed water resonance area;  $N1H_{met}$  demonstrates the number of the equivalent proton in the metabolite groups;  $W_{conc}$  is the water concentration in the measured MRS voxel in mM/L;  $att_{met}$  and  $ATT_{H2O}$  are the attenuation factor of the respective metabolite and water.

# 3

## **Comparing Gln/Glu Separation Using STEAM with Short and Long TE/TM at 3 and 7 T**

# Comparing Gln/Glu Separation Using STEAM with Short and Long TE/TM at 3 and 7 T

---

## 3.1 Preface

The goal in this chapter is to determine the optimal echo time (TE) / mixing time (TM) setting in stimulated-echo acquisition mode (STEAM) for *in vivo* glutamine (Gln) and glutamate (Glu) acquisitions and separation at 7 T.

Glutamate is the major excitatory neurotransmitter in the central nervous system. Glutamine, the precursor of Glu, is synthesized from Glu in astrocytes and converted into Glu after released into neurons (Albrecht et al., 2010; Daikhin and Yudkoff, 2000). Accurate detection of *in vivo* Glu and Gln is of particular interest in clinical field (Yang et al., 2008), as the concentration levels of Glu and the Glu/Gln ratio are closely linked to many neurological and psychiatric diseases, including Alzheimer's dementia (Moats et al., 1994), Huntington's disease (Taylor-Robinson et al., 1996) and major depressive disorder (Horn et al., 2010). However, due to the similar chemical shifts and J-coupling effects, Gln and Glu spectra are severely overlapped and thus the reliable detection of both metabolites is largely limited (Yang et al., 2008).

As one widely applied proton magnetic resonance spectroscopy ( $^1\text{H}$ -MRS) technique, STEAM is considered being feasible to effectively and efficiently measure Gln and Glu spectra in parallel (Graaf and Rothman, 2001; Bartha et al., 2000; Tkáč et al., 2001). Since spectral responses of Gln and Glu in STEAM are highly varied according to the choices of field-specific inter-pulse timings, i.e., TE and TM (Thompson and Allen, 2001), Yang et al., (2008) systematically simulated the STEAM spectra of Gln and Glu with a range of TEs and TMs for 3 T to 9.4 T and found field-specific long TE/TM settings to optimally resolve Gln and Glu signals of the Carbon-4 (C4) proton resonances, which are the main spectral peaks of Gln and Glu. In the mean while, STEAM with short TE/TM was also suggested to acquire Gln and Glu at strong field strengths, since high signal-to-noise-ratio (SNR) at short TE and increased chemical shift dispersion at strong field strengths for partially resolving spectral overlap problem can largely benefit the Gln and

## Comparing Gln/Glu Separation Using STEAM with Short and Long TE/TM at 3 and 7 T

---

Glu acquisitions (Bartha et al., 2000; Tkáč et al., 2001). Moreover, Stephan et al., (2011) estimated *in vivo* Gln and Glu acquired using STEAM with short TE/TM (16 ms / 17 ms) and 7 T-specific long TE/TM (74 ms / 68 ms; Yang et al., 2008) at 7 T. They found significantly lower Cramer-Rao lower bound (CRLB) values of the Gln and Glu at short TE/TM.

Based on these previous studies, it is however still unclear whether the optimal spectral separation between Gln and Glu and thus the accurate concentration quantification can be achieved by field-specific long TE/TM or the higher spectral SNR at short TE/TM. Therefore, to determine the optimal TE/TM for Gln and Glu acquisitions and quantification, a comparison study is implemented in this chapter to systematically compare the Gln and Glu signals acquired using STEAM with short and field-specific long TE/TM at 3 and 7 T.

This chapter firstly introduces the basic knowledge of Gln and Glu including their chemical structures and properties of each group and explains that why spectral patterns of Gln and Glu are strongly influenced by different options of TE and TM values in STEAM. Secondly, this chapter describes the acquisitions of Gln and Glu signals in simulations, in a man-made phantom and in healthy human brains using STEAM with short TE/TM (20 ms / 10 ms) and proposed field-specific long TE/TM settings (72 ms / 6 ms for 3 T; 74 ms / 68 ms for 7 T; Yang et al., 2008) at 3 and 7 T. Besides to the CRLB estimations for Gln and Glu, the detailed concentration relationships and the degrees of correlation between Gln and Glu are also taken into account. Additionally, point-resolved spectroscopy (PRESS) with short TE of 35ms is also applied to acquire *in vivo* spectra in 3 T, in order to further investigate the relationship between high SNR and quantification of Gln and Glu.

## 3.2 Background

### 3.2.1 Glutamate and Glutamine

Glutamate (Fig. 3.1.A) is an amino acid with an acidic side chain. It is found as the most abundant amino acid in human brain with a concentration of approximately 12mmol/kg<sub>ww</sub> (Govindaraju et al., 2000). Glutamate has two methylene groups and a methine group that are strongly J-coupled, giving rise to a complex spectrum with multiplets (Govindaraju et al., 2000). As measured by Govindaraju et al., (2000), the signal from the single proton of the methine group is spread over as a doublet-of-doublets which are centering at 3.74 ppm, while the resonances of the two methylene group are closely grouped in the range of 2.04 to 2.35 ppm.

Glutamine (Fig. 3.1.B) is structurally similar to glutamate with two methylene groups and a methine group, and its coupling pattern is the same as Glu. A triplet from the methine proton resonates at 3.75 ppm. The multiplets from the four methylene protons are closely grouped from 2.12 to 2.46 ppm. The two amide protons appear at 6.82 and 7.53 ppm as they are chemically nonequivalent (Govindaraju et al., 2000).

In the central nervous system, Gln, as the precursor of Glu, is synthesized in astrocytes from Glu. Then, Glu is released by neurons and re-uptaken by astrocytes with the conversion back to Gln (Pfleiderer et al., 2003). Due to the very close chemical shifts, the spectra of Gln and Glu are partially overlaid and reported to be very difficult to separate. Therefore, the contributions of Gln and Glu are commonly combined and denoted as 'Glx' when analyzing *in vivo* spectra.

The detailed values of chemical shifts and J-couplings, types of multiplicity and other chemical structure parameters for Gln and Glu are provided in Table 3.1.

## Comparing Gln/Glu Separation Using STEAM with Short and Long TE/TM at 3 and 7 T

---

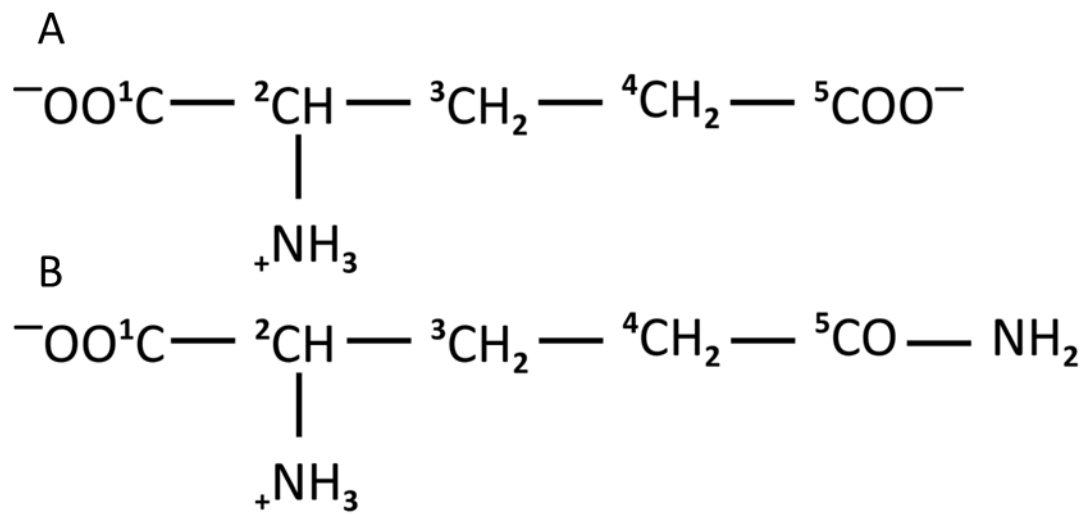


**Figure 3.1** The chemical structures of glutamate (A) and glutamine (B) (Govindaraju et al., 2000).

## Comparing Gln/Glu Separation Using STEAM with Short and Long TE/TM at 3 and 7 T

**Table 3.1** The chemical shifts and J-coupling values for glutamate and glutamine. Chemical shifts are reported with reference to DSS-trimethyl singlet resonance at 0.0 ppm, and multiplicity definitions are: d, doublet; t, triplet; m, other multiplet (Govindaraju et al., 2000).

Compound	Group	Chemical Shift (ppm)	Multiplicity	J-Coupling	Connectivity
Glutamate	<sup>2</sup> CH	3.7433	dd	7.331	2 – 3
	<sup>3</sup> CH <sub>2</sub>	2.0375	m	4.651	2 – 3'
		2.1200	m	-14.849	3 – 3'
	<sup>4</sup> CH <sub>2</sub>	2.3378	m	8.406	3 – 4'
		2.3520	m	6.875	3' – 4'
				6.413	3 – 4
				8.478	3' – 4
			-15.915	4 – 4'	
Glutamine	<sup>2</sup> CH	3.7530	t	5.847	2 – 3
	<sup>3</sup> CH <sub>2</sub>	2.1290	m	6.500	2 – 3'
		2.1090	m	-14.504	3 – 3'
	<sup>4</sup> CH <sub>2</sub>	2.4320	m	9.165	3 – 4
		2.4540	m	6.347	3 – 4'
				6.324	3' – 4
				9.209	3' – 4'
			-15.371	4 – 4'	

### 3.2.2 Effect of TE/TM on Gln and Glu

As reported by Thompson and Allen (2001), the spectral patterns of strongly coupled spin systems Gln and Glu are strongly depended on the choice of two inter-pulse times (i.e., TE and TM) in a STEAM sequence, since both TE and TM can affect the time-dependent intermediate states of magnetization, i.e., anti-phase coherence and zero quantum coherence. Both inter-pulse evolutions can influence the magnitude of components that eventually contribute to the observable line shape.

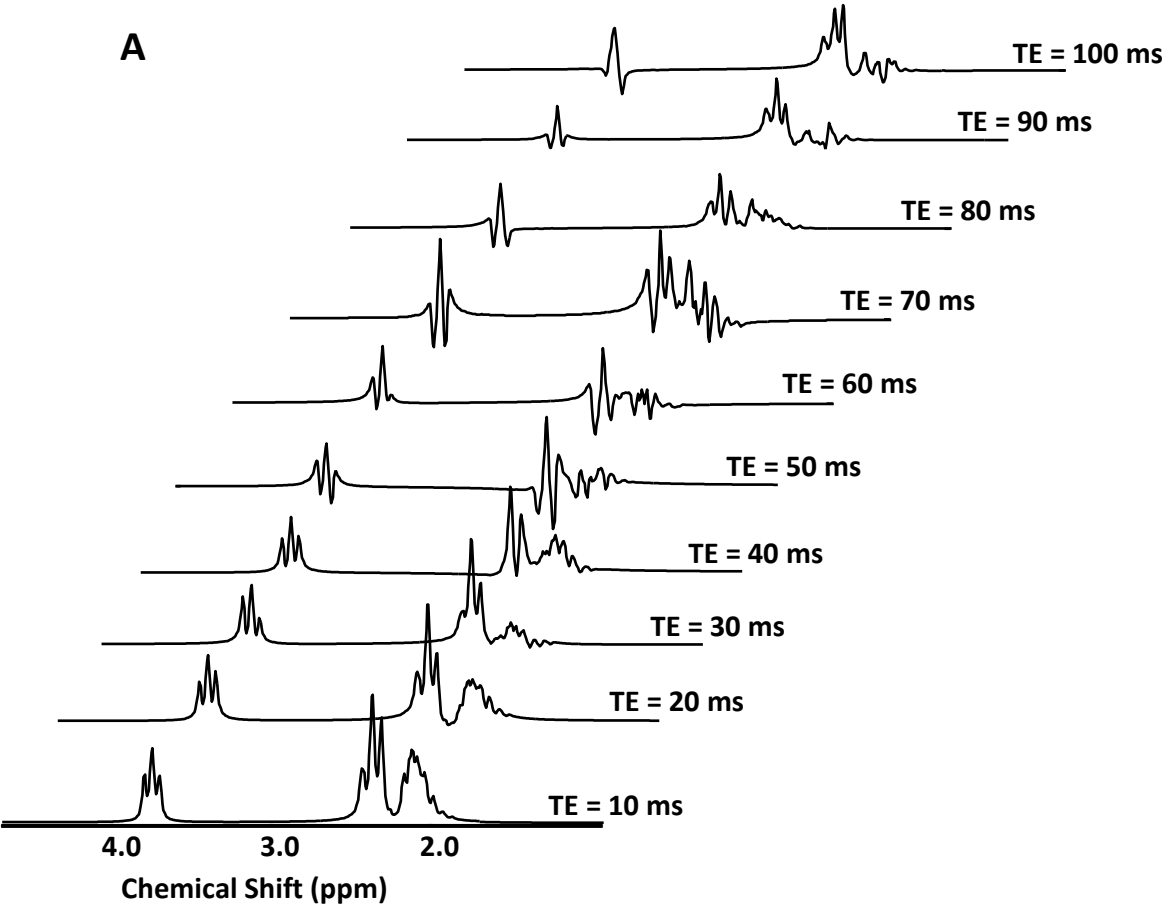
## Comparing Gln/Glu Separation Using STEAM with Short and Long TE/TM at 3 and 7 T

---

In a standard STEAM sequence (Fig. 2.2.B), after the first  $90^\circ$  excitation pulse, the mixture of in-phase coherence and zero quantum coherence evolve from in-phase evolution transverse magnetization during the first TE/2 period. The evolution is primarily governed by J-coupling constants of Gln and Glu (Table 3.1). After the second  $90^\circ$  pulse, the resulted in-phase coherences at the end of the first TE/2 are transformed to longitudinal magnetization and the anti-phase coherences are converted into multiple quantum coherences. The magnitude of the anti-phase coherences is dominated by the choice of TE. Among the yielded multiple quantum coherences, all high order quantum terms are dephased by TM spoiler gradients and only the gradient-insensitive zero quantum terms oscillate during the TM period. The zero quantum coherences evolve between real and imaginary states and the longitudinal terms keep static. After the final third  $90^\circ$  pulse, the longitudinal magnetization is flipped back to the transverse plane into both in- and anti-phase coherences, and only the TM-dependent imaginary part of the zero quantum coherences are transformed to anti-phase coherence due to the phase-sensitivity of this process. After the final TE/2 evolution period, both in- and anti-phase coherences evolve into the final mixture of transverse coherences and determine the metabolite line shape.

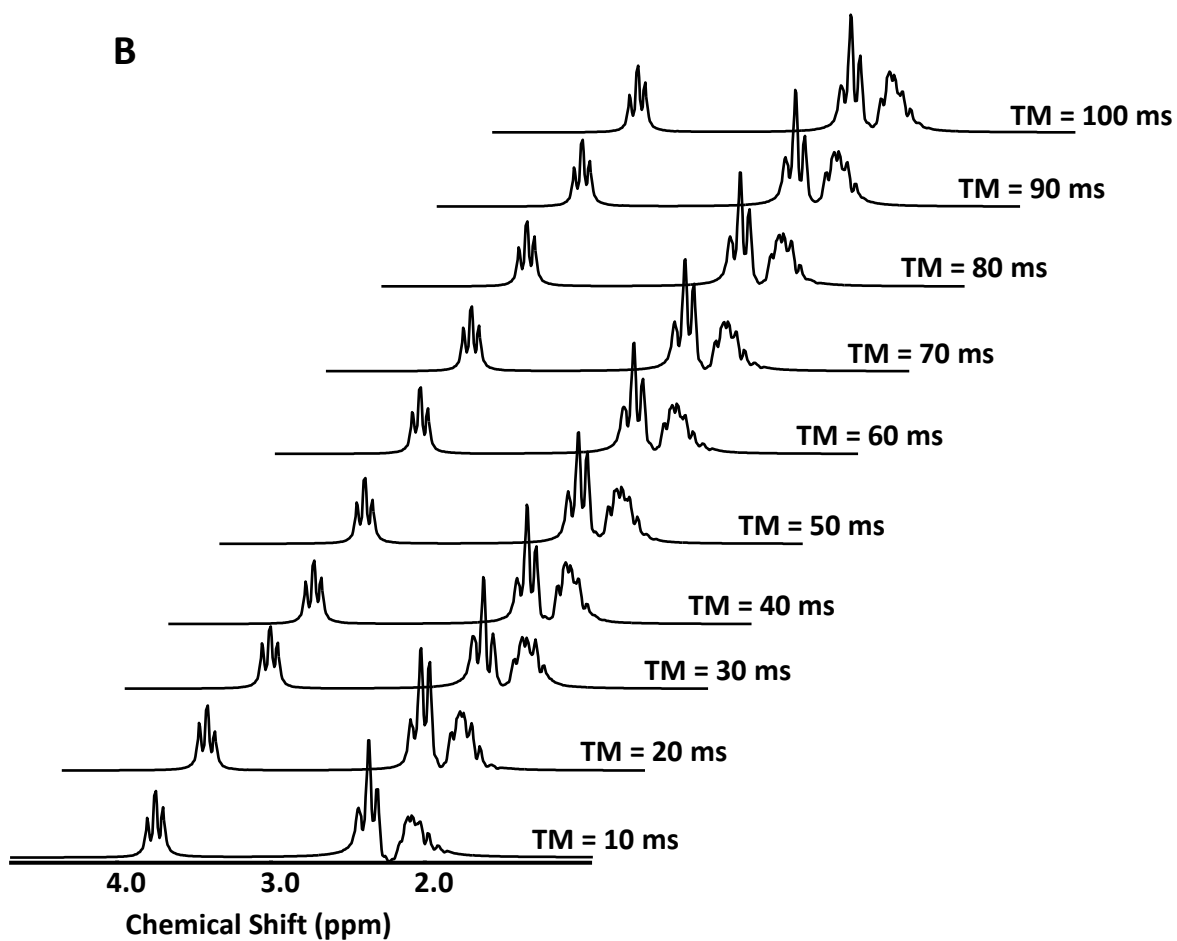
As an example, the simulated spectral responses of Glu in STEAM acquisition with different TEs and TMs are shown in Fig. 3.2.

# Comparing Gln/Glu Separation Using STEAM with Short and Long TE/TM at 3 and 7 T

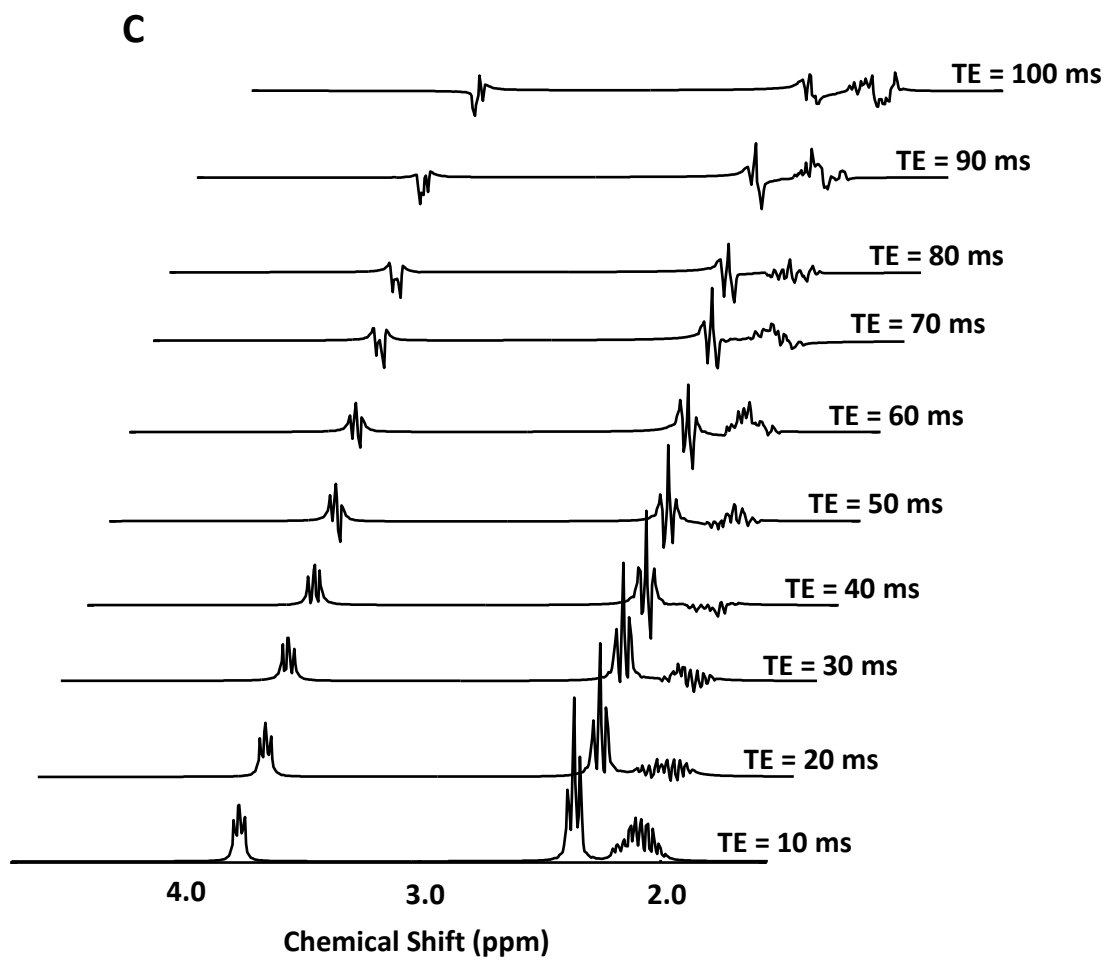


# Comparing Gln/Glu Separation Using STEAM with Short and Long TE/TM at 3 and 7 T

---



# Comparing Gln/Glu Separation Using STEAM with Short and Long TE/TM at 3 and 7 T



## Comparing Gln/Glu Separation Using STEAM with Short and Long TE/TM at 3 and 7 T

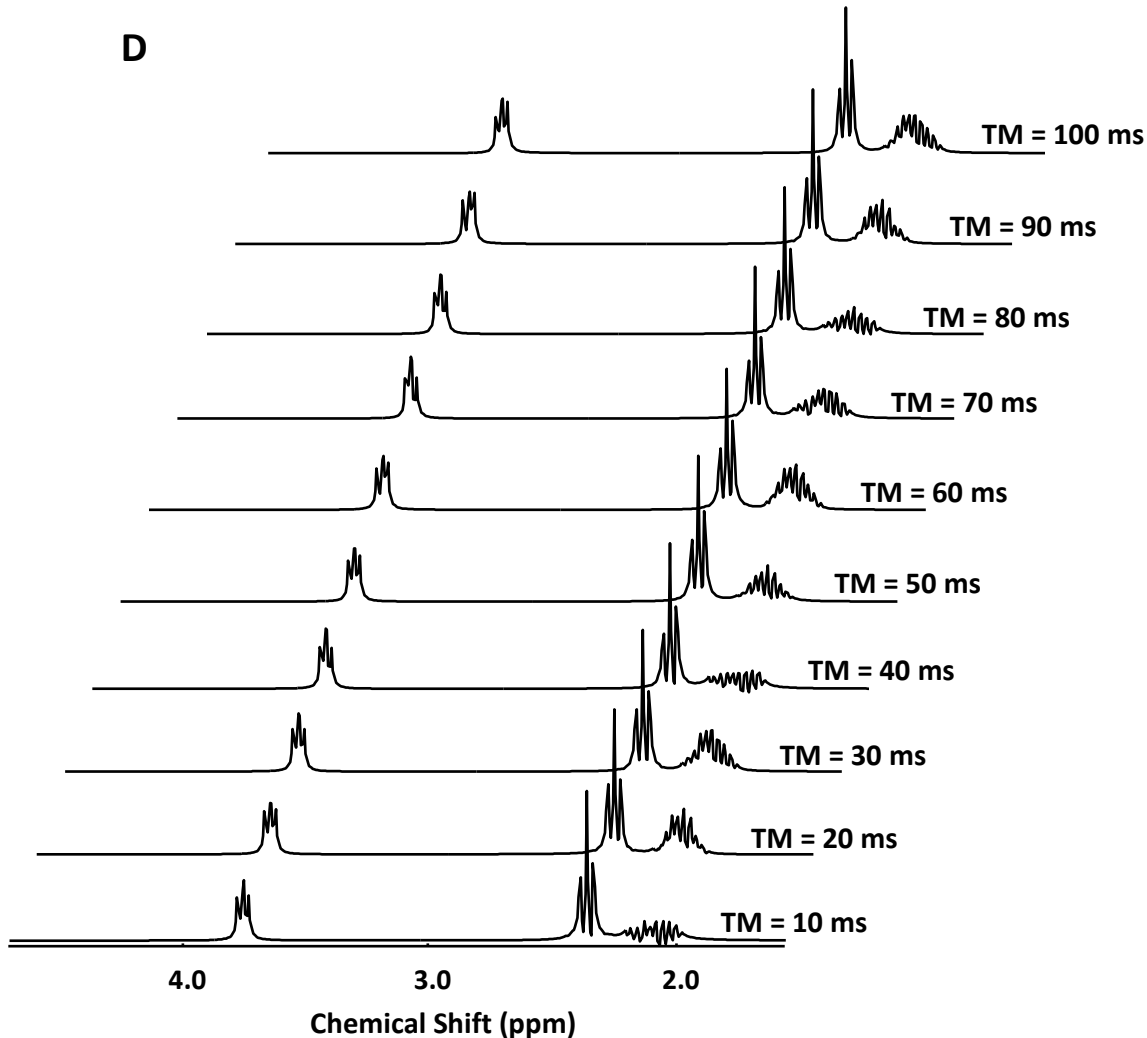


**Figure 3.2** Simulated spectral responses of Glu in STEAM acquisition with fixed TM of 10 ms and TEs of 10 ms to 100 ms with an increased step of 10 ms under field strengths of 3 T (A) and 7 T (C), and with fixed TE of 20 ms and varied TMs from 10 ms to 100 ms with 10 ms increased step under field strengths of 3 T (B) and 7 T (D).

## Comparing Gln/Glu Separation Using STEAM with Short and Long TE/TM at 3 and 7 T

---

### 3.3 Materials and Methods

#### 3.3.1 Spectral Simulation for Gln and Glu

The software *Versatile Simulation, Pulses and Analysis for Magnetic Resonance Spectroscopy* (VeSPA) version 0.7.1, developed according to the GAMMA/PyGAMMA NMR simulation libraries (Smith et al., 1994; Soher et al., 2013), was applied to simulate the STEAM spectra of Gln or Glu at short and long TE/TM settings at 3 and 7 T. The chemical shift values and J-coupling constants of Gln and Glu were obtained from Govindaraju et al., (2000). The field strengths, short and long TE/TM values were separately set as 123.26 MHz, 20 ms / 10 ms and 72 ms / 6 ms for 3 T and 297.14 MHz, 20 ms / 10 ms and 74 ms / 68 ms for 7 T, in which the field-specific long TE/TM settings were proposed by Yang et al., (2008). The embedded standard STEAM sequence with ideal hard 90°-90°-90° RF pulses was selected to simulate spectra for simplicity, since the choice of realistic or ideal hard selective 90° pulse was demonstrated not a critical factor governing spectral responses in STEAM acquisition (Thompson and Allen, 2001).

#### 3.3.2 Phantom Results

A spherical phantom (40 mm diameter) was used in phantom experiments, containing 100 mM Glu and 17 mM Gln in a buffered solution (pH = 7.2). The concentration ratio of Glu to Gln (Glu/Gln) is 5.88, aiming to agree with the recently proposed Glu/Gln ratio in human posterior cingulate cortex (PCC) region (Dou et al., 2013).

All phantom experiments were performed using a 3 T Siemens MAGNETOM Trio scanner with an 8 channel phased-arrayed head coil and a 7 T MR scanner (Siemens MAGNETOM) with a 32-channel head array coil. To acquire  $T_1$ -weighted phantom images, three dimensional (3D) magnetization-prepared rapid gradient echo (MPRAGE) sequence with image resolution of 1.0 x 1.0 x 2.0 mm<sup>3</sup> was applied at 3 T with TE = 5.01 ms, repetition

## Comparing Gln/Glu Separation Using STEAM with Short and Long TE/TM at 3 and 7 T

time (TR) = 1650 ms, inversion time (TI) = 1100 ms, flip angle (FA) = 7°, bandwidth (BW) = 130 Hz/pixel and acquisition matrix = 256 x 256 x 96. A separate 1.0 mm resolution isotropic 3D MPRAGE sequence was applied at 7 T using TE = 2.66 ms, TR = 2300 ms, TI = 1050 ms, FA = 5°, BW = 150 Hz/pixel and acquisition matrix = 256 x 256 x 192. Based on these high resolution images, all MR spectroscopy (MRS) voxels were placed in the phantom center and manually shimmed to optimize magnetic field homogeneity by the vendor-provided automatic shim procedure. After these voxel-wise adjustments, a standard STEAM (128 averages, TR = 2000 ms, short TE/TM = 20 ms / 10 ms and long TE/TM = 72 ms / 6 ms, voxel size = 15 x 15 x 15 mm<sup>3</sup>, data size = 2048 points, BW = 2000 Hz) was employed to acquire phantom spectra at 3 T. The spectrum acquisition for each region took four minutes and twenty four seconds. STEAM with variable rate selective excitation (VERSE) pulses was applied to acquire phantom spectra at 7 T with 128 averages, TR = 3000 ms, short TE/TM = 20 ms / 10 ms and long TE/TM = 74 ms / 68 ms, voxel size = 10 x 10 x 10 mm<sup>3</sup>, data size = 2048 points and BW = 2800 Hz. The acquisition time for each region was six minutes and thirty six seconds. The application of VERSE pulses aimed to reduce the peak power requirements of RF pulses at high field strength (Elywa et al., 2012). Corresponding water reference spectra for eddy current correction and absolute metabolite concentration quantification were also acquired at 3 and 7 T.

### 3.3.3 *In Vivo* Results

Fourteen healthy male subjects were recruited for human brain scans. Of these subjects, six (28 ± 4 years old) were selected for 3 T scans, and the remaining eight (26 ± 3 years old) were measured at 7 T. To rule out present physical illness and psychiatric abnormality, all subjects were assessed before participation using self-report questionnaires approved by the local ethical committee according to the declaration of Helsinki.

## Comparing Gln/Glu Separation Using STEAM with Short and Long TE/TM at 3 and 7 T

---

Similar to the phantom measurements, the human experiments were performed in the same 3 T system with an 8-channel head coil and in the same 7 T system albeit with a 24-channel head array coil. A 1.0 mm resolution isotropic 3D MPRAGE sequence was applied for 3 T  $T_1$ -weighted anatomical image acquisitions with TE = 4.77 ms, TR = 2500 ms, TI = 1100 ms, FA = 7°, BW = 140 Hz/pixel and acquisition matrix = 256 x 256 x 192. A 0.8 mm resolution isotropic 3D MPRAGE sequence was employed for acquiring 7 T  $T_1$ -weighted brain anatomical images with TE = 2.73 ms, TR = 2300 ms, TI = 1050 ms, FA = 5°, BW = 150 Hz/pixel and acquisition matrix = 320 x 320 x 224. A reconstruction of MPRAGE images was implemented into the anterior commissure – posterior commissure plane providing the anterior – posterior direction for MRS voxel positioning. Based on the reconstructed MPRAGE images, MRS voxels with voxel size 25 x 15 x 10 mm<sup>3</sup> = 3.75 ml were placed in the rostral PCC (rPCC) region (Fig. 3.3.A) for all 3 and 7 T subjects, as well as an additional caudal PCC (cPCC) region (Fig. 3.3.B) for 3 T subjects. Local  $B_1$  adjustments were applied to improve the magnetic field homogeneity for voxel-specific regions at 3 and 7 T. The STEAM and STEAM VERSE sequences with identical TR/TE/TM settings, as in the phantom experiments, were separately applied for *in vivo* spectrum acquisitions at 3 and 7 T. In addition, PRESS sequences (128 averages, TR = 2000 ms, short TE = 35 ms, voxel size = 25 x 15 x 10 mm<sup>3</sup> = 3.75 ml, data size = 2048 points, BW = 2000 Hz) were employed at 3 T. The spectrum acquisition took four minutes and twenty four seconds for each voxel.

## Comparing Gln/Glu Separation Using STEAM with Short and Long TE/TM at 3 and 7 T

---

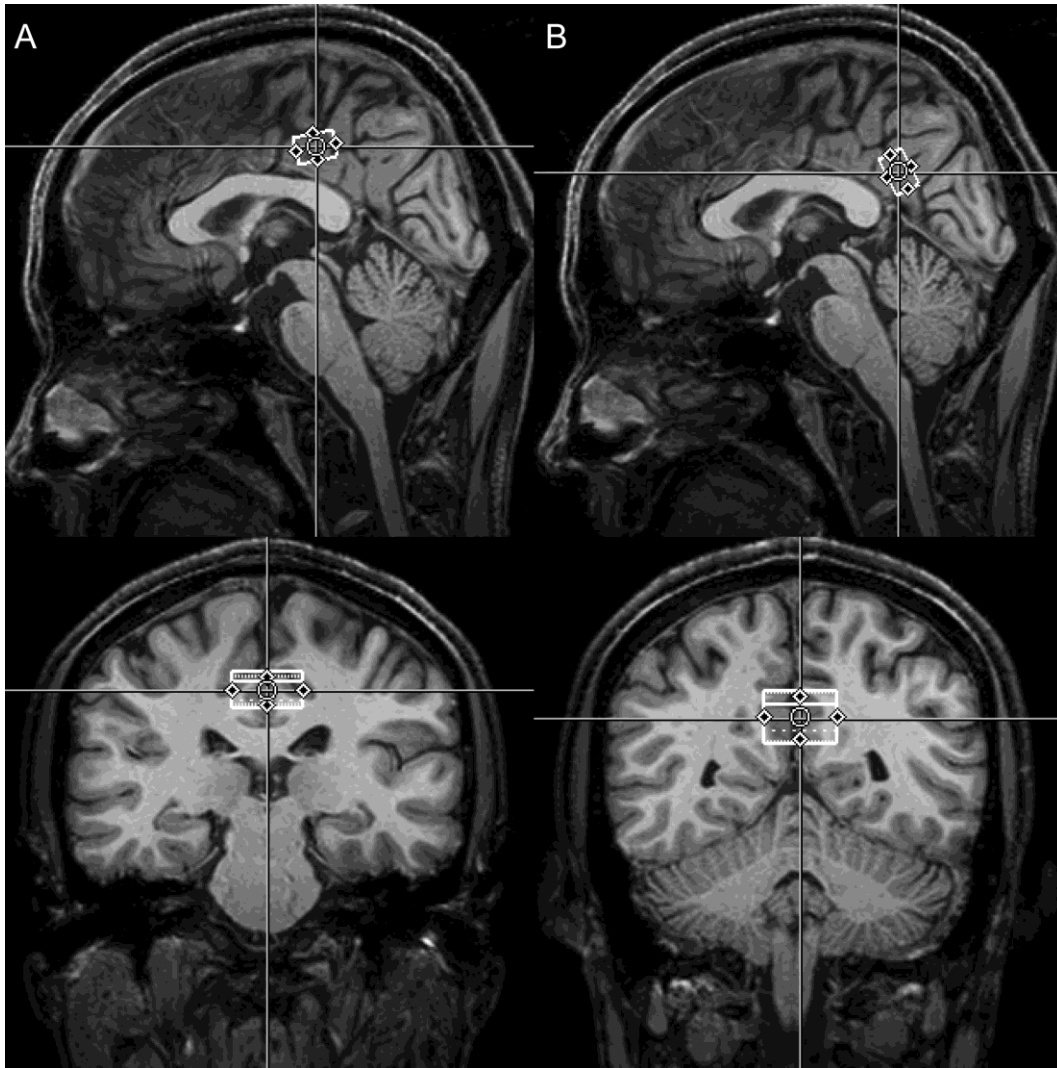


**Figure 3.3** Voxel placement in the rPCC region (A) and cPCC region (B) in representative 3D MPRAGE anatomical images acquired at 3 T.

### 3.3.4 Basis Set Making

Four TE/TM- and field-specific basis sets for analyzing *in vivo* spectra consist of measured Gln and Glu spectra and fifteen simulated spectra of alanine, aspartate, N-acetylaspartate (NAA), N-Acetylaspartylglutamic acid, choline, creatine (Cr), GABA, glucose, glycerophosphocholine, glutathione, myo-Inositol, phosphocreatine, lactate,

## Comparing Gln/Glu Separation Using STEAM with Short and Long TE/TM at 3 and 7 T

phosphocholine, and scyllo-inositol. Gln and Glu spectra were measured using STEAM with identical TR/TE/TM as in the phantom measurements at 3 T and 7 T. All other metabolite spectra were simulated using VeSPA version 0.7.1 with the same parameter settings as explained in section 3.3.1. The corresponding J-coupling and chemical shift values of metabolites were acquired from Govindaraju et al., (2000).

To analyze *in vivo* spectra acquired using short TE PRESS, the sequence-specific *in vitro* spectra basis set was measured with identical TR/TE at 3 T. It includes sixteen major metabolite spectra (alanine, aspartate, NAA, N-Acetylaspartylglutamic acid, Cr, GABA, Glu, Gln, glucose, glycerophosphocholine, glutathione, myo-Inositol, phosphocreatine, lactate, phosphocholine, and taurine).

### 3.3.5 Data Analysis

The spectral overlap between simulated Gln and Glu spectra were assessed by calculating the geometrical overlap ratios as the Gln and Glu intersection relative to the set union of Gln and Glu ( $Gln \cap Glu / Gln + Glu$ ) in the range of 2.25 ppm to 2.55 ppm. The SNRs of phantom and *in vivo* spectra were respectively calculated according to the equations of  $SNR_{phantom} = \text{Peak Height of Glu} / \text{standard deviation of spectral noise}$  and  $SNR_{in vivo} = \text{Peak Height of NAA} / \text{standard deviation of spectral noise}$ .

LCModel version 6.1.0 (Provencher, 1993) was applied to analyze all phantom and *in vivo* spectra. Full width at half maximum (FWHM) values for spectral line-width estimation, the absolute metabolite concentrations with respective CRLBs and correlation coefficients between Gln and Glu were obtained. Because the  $T_1$  and  $T_2$  relaxation effects of metabolites can severely influence the metabolite quantification especially at long TE and TM (Provencher, 2013, 128-129), the correction for relaxation effects was taken into account when using LCModel for metabolite quantification. For

## Comparing Gln/Glu Separation Using STEAM with Short and Long TE/TM at 3 and 7 T

simplicity, the field-specific  $T_1$  and  $T_2$  values of Cr (the reference metabolite in LCMoDel analysis) were used: 1380 ms and 151 ms for 3 T and 1760 ms and 121 ms for 7 T (Li et al., 2008). The metabolite concentrations were expressed using institutional units (i.u.).

*In vivo* spectra with poor quality were excluded, following standard criteria of SNR < 15, FWHM > 12 Hz (for 3 T) and > 25 Hz (for 7 T), CRLBs for Gln+Glu (Glx), Gln and Glu > 100% (Stephan et al., 2011; Tkáč et al., 2009). In total, two Gln values were discarded from the whole data sample, corresponding to less than 2% of all entries. The missing values were replaced by mean levels of respective Gln data. Additionally, the paired t-tests toolbox in SPSS 18 (SPSS for Windows, Chicago III, USA) was applied for the full sample to test the significance with the significance threshold of  $p = 0.05$ . The 3 T rPCC and cPCC spectra were combined as PCC spectra for paired t-test analysis, since the Gln and Glu concentrations in both sub-regions of PCC were reported to have no significant difference (Dou et al., 2013).

### 3.4 Results

#### 3.4.1 Simulation Results

Simulated Gln and Glu spectra are shown in Fig. 3.4. At 3 T, the geometrical overlap ratio  $Gln \cap Glu / Gln + Glu$  for Gln and Glu (Fig. 3.4.A, B) using short TE/TM was 6% larger than that using long TE/TM (28% vs 22%). At increased field strength of 7 T, the spectral separation between the simulated Gln and Glu is higher using either short or long TE/TM (Fig. 3.4.C, D). The corresponding overlap ratio for Gln and Glu with short TE/TM was slightly larger than that with long TE/TM (11% vs 10%).

## Comparing Gln/Glu Separation Using STEAM with Short and Long TE/TM at 3 and 7 T

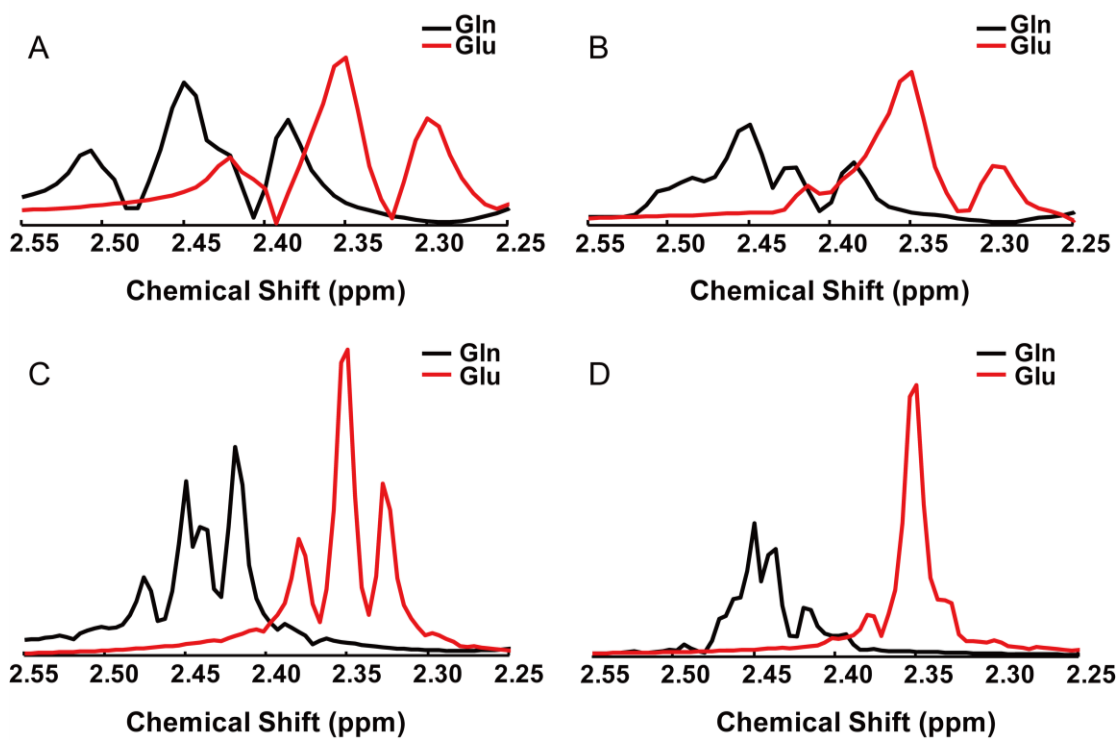


**Figure 3.4** Simulated STEAM spectra of Glu (red) and Gln (black) of the C4 proton resonances (around 2.35 ppm for Glu and 2.45 ppm for Gln) with short TE/TM (20 ms / 10 ms; A) and long TE/TM (72 ms / 6 ms; B) at 3 T, and with short TE/TM (20 ms / 10 ms; C) and long TE/TM (74 ms / 68 ms; D) at 7 T.

### 3.4.2 Phantom Results

Fig. 3.5 and Table 3.2 show the phantom results. The Glu/Gln concentration ratios using long TE/TM reflected the true value 5.88 more accurately than those using short TE/TM at 3 and 7 T (3 T: 6.86 vs 8.64; 7 T: 5.87 vs 5.99), although short TE/TM provided higher SNRs and less CRLBs than long TE/TM.

## Comparing Gln/Glu Separation Using STEAM with Short and Long TE/TM at 3 and 7 T

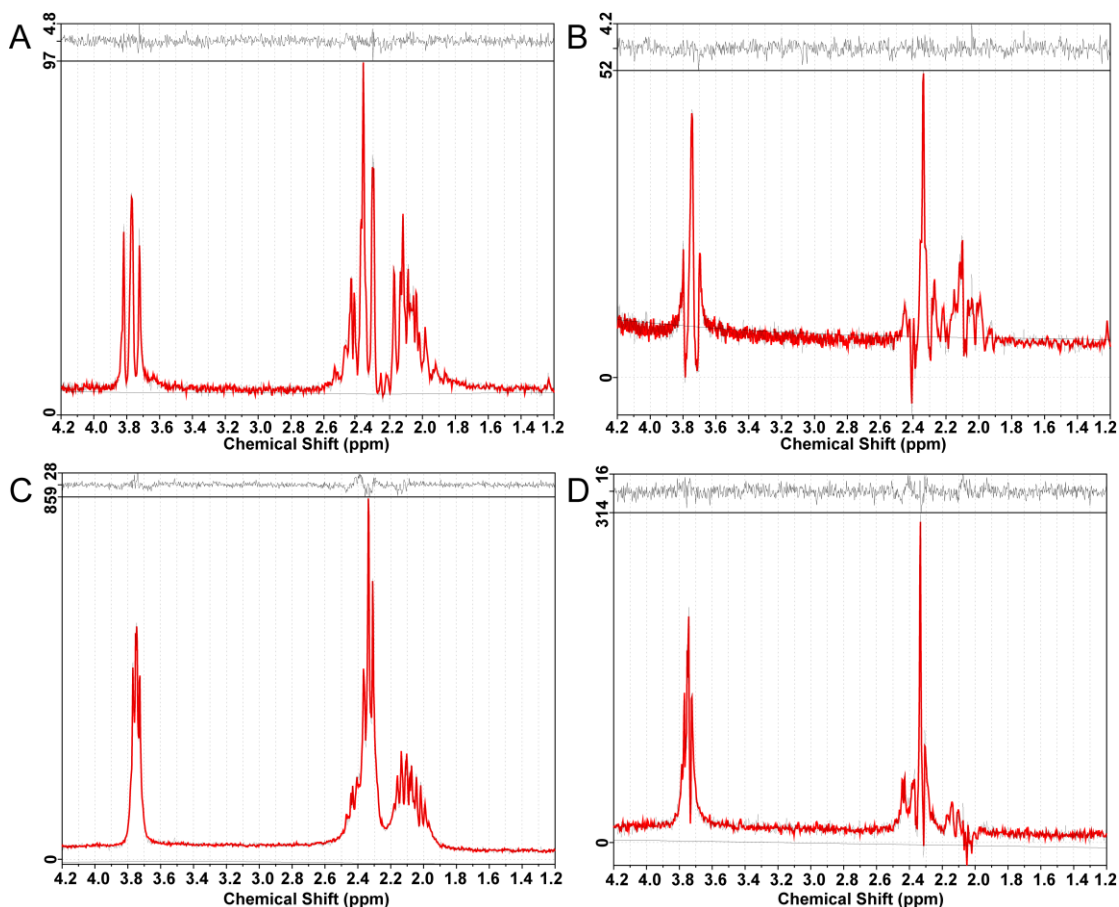


**Figure 3.5** LCMoel analyzed phantom spectra: A and B show the spectra acquired using STEAM with short TE/TM (20 ms / 10 ms) and long TE/TM (72 ms / 6 ms) at 3 T; C and D show the spectra acquired using STEAM with VERSE at short TE/TM (20 ms / 10 ms) and long TE/TM (74 ms / 68 ms) at 7 T.

**Table 3.2** Quantitative phantom results from STEAM acquisitions with short and long TE/TM (20 ms / 10 ms & 72 ms / 6 ms) at 3 T and STEAM with VERSE (20 ms / 10 ms & 74 ms / 68 ms) at 7 T.

	Short TE/TM				Long TE/TM			
	SNR	CRLB (%)			SNR	CRLB (%)		
		Glu/Gln	Gln	Glu		Glu/Gln	Gln	Glu
3T	134	8.64	4	1	83	6.86	7	1
7T	270	5.99	2	0	147	5.87	4	1

## Comparing Gln/Glu Separation Using STEAM with Short and Long TE/TM at 3 and 7 T

---

### 3.4.3 *In Vivo* Results

#### 3 T

All 3 T spectra (Fig. 3.6.A, B, C) were compared using paired t-tests. No significant difference for spectral FWHMs were revealed between short TE/TM and long TE/TM ( $4.0 \pm 0.7$  Hz vs  $4.1 \pm 0.6$  Hz;  $T = -0.77$ ,  $p = 0.46$ ), between short TE/TM and PRESS ( $4.0 \pm 0.7$  Hz vs  $4.3 \pm 0.5$  Hz;  $T = -1.34$ ,  $p = 0.21$ ), and between long TE/TM and PRESS ( $4.1 \pm 0.6$  Hz vs  $4.3 \pm 0.5$  Hz;  $T = -1.00$ ,  $p = 0.34$ ).

Significantly higher SNRs were found in the spectra acquired using PRESS than those using STEAM with short TE/TM ( $60 \pm 10$  vs  $40 \pm 5$ ;  $T = 6.42$ ,  $p < 0.001$ ), while the SNRs of spectra measured using STEAM with short TE/TM were significantly higher than those with long TE/TM ( $40 \pm 5$  vs  $30 \pm 3$ ;  $T = 7.62$ ,  $p < 0.001$ ).

As shown in Table 3.3, Glx concentrations have not shown significant difference between short and long TE/TM ( $T = -0.07$ ,  $p = 0.95$ ), between long TE/TM and PRESS ( $T = -2.13$ ,  $p = 0.06$ ), although marginal difference was found between short TE/TM and PRESS ( $T = -2.35$ ,  $p = 0.04$ ). However, significantly different spectral separation between Gln and Glu were found between short and long TE/TM (Gln:  $T = -5.84$ ,  $p < 0.001$ ; Glu:  $T = 6.05$ ,  $p < 0.001$ ), between short TE/TM and PRESS (Gln:  $T = 2.62$ ,  $p = 0.02$ ; Glu:  $T = -6.74$ ,  $p < 0.001$ ), and between long TE/TM and PRESS (Gln:  $T = 8.79$ ,  $p < 0.001$ ; Glu:  $T = -13.3$ ,  $p < 0.001$ ).

Comparable correlation coefficients between Gln and Glu (Table 3.3) were found between short and long TE/TM ( $T = 0.70$ ,  $p = 0.50$ ), and between short TE/TM and PRESS ( $T = -1.61$ ,  $p = 0.14$ ), while significantly different correlation coefficients between Gln and Glu were observed between long TE/TM and PRESS ( $T = -2.47$ ,  $p = 0.03$ ).

## Comparing Gln/Glu Separation Using STEAM with Short and Long TE/TM at 3 and 7 T

---

### 7 T

Significantly higher SNRs were found in the spectra using short TE/TM than those using long TE/TM ( $132 \pm 31$  vs  $78 \pm 17$ ;  $T = 5.80$ ,  $p = 0.001$ ), and the FWHM values were statistically identical between short and long TE/TM ( $8.2 \pm 1.9$  Hz vs  $9.4 \pm 2.0$  Hz;  $T = -2.05$ ,  $p = 0.08$ ).

As shown in Fig. 3.6.D, E and Table 3.3, short TE/TM showed no significantly different Glx concentrations but different separation between Gln and Glu compared to long TE/TM (Glx:  $T = 0.06$ ,  $p = 0.95$ ; Gln:  $T = 5.74$ ,  $p = 0.001$ ; Glu:  $T = -2.57$ ,  $p = 0.04$ ), and significantly lower correlation than long TE/TM ( $T = 7.00$ ,  $p < 0.001$ ).

## Comparing Gln/Glu Separation Using STEAM with Short and Long TE/TM at 3 and 7 T

---

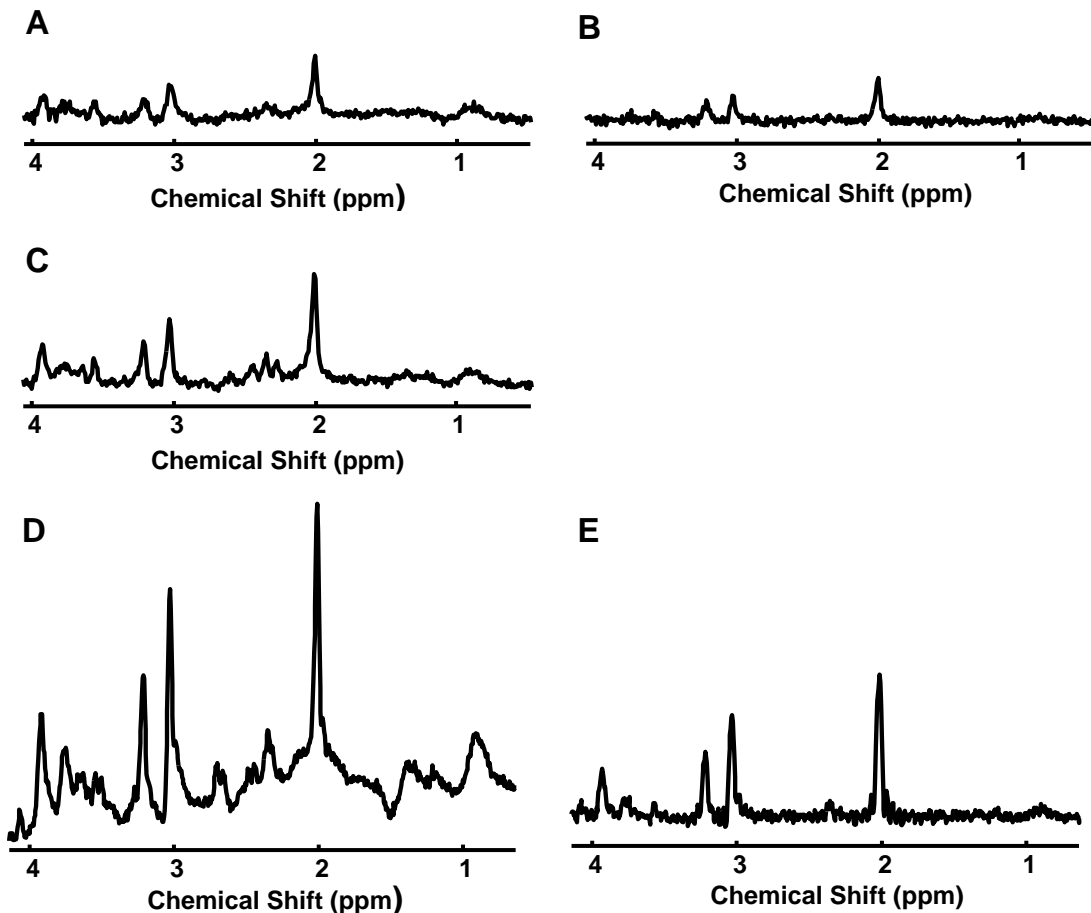


**Figure 3.6** Example 3 T *in vivo* spectra from the cPCC region using STEAM with short TE/TM (20 ms / 10 ms; A), long TE/TM (72 ms / 6 ms; B) and using PRESS with short TE 35 ms (C), and 7 T *in vivo* spectra from the rPCC region using STEAM with VERSE with short TE/TM (20 ms / 10 ms; D) and long TE/TM (74 ms / 68 ms; E).

## Comparing Gln/Glu Separation Using STEAM with Short and Long TE/TM at 3 and 7 T

**Table 3.3** Quantitative results from the *in vivo* measurements: At 3 T, all *in vivo* Gln and Glu signals were measured in the PCC region using STEAM with short and long TE/TM (20 ms / 10 ms & 72 ms / 6 ms) and PRESS with TE 35 ms; At 7 T, all *in vivo* Gln and Glu signals were acquired in the rPCC region using STEAM with VERSE with short and long TE/TM (20 ms / 10 ms & 74 ms / 68 ms). Absolute concentrations are expressed using institutional units (i.u.).

TE/TM or TE (ms)	Glx		Glu		Gln		Corr.Coef.	
	CRLB	Abs.Con.	CRLB	Abs.Con.	CRLB	Abs.Con.		
	(%)	(i.u.)	(%)	(i.u.)	(%)	(i.u.)		
3T	20 / 10	12.3±1.5	12.6±0.9	13.1±1.4	8.8±1.0	30.5±8.6	3.7±0.9	-0.08±0.05
	72 / 6	18.5±5.1	12.6±1.7	28.0±8.1	6.3±1.2	26.5±9.5	6.3±1.3	-0.10±0.07
	35	9.6±1.3	13.4±1.1	9.9±1.2	10.5±0.7	29.3±7.2	2.9±0.7	-0.05±0.03
7T	20 / 10	3.8±0.7	8.4±1.0	3.8±0.7	7.2±0.7	14.9±3.0	1.2±0.3	-0.04±0.02
	74 / 68	7.1±1.0	8.4±0.9	6.5±0.9	8.0±0.8	75.3±24.9	0.5±0.2	-0.12±0.05

### 3.5 Discussion

In this study, STEAM spectra of Gln and Glu at short and field-specific long TE/TM were simulated, and the corresponding *in vitro* and *in vivo* Gln and Glu signals were measured at 3 and 7 T. These acquired Gln and Glu signals with short TE/TM for high SNR and with field-specific long TE/TM for best separating main peaks of Gln and Glu were analyzed and compared to determine the optimal TE/TM setting for Gln and Glu acquisitions and separation.

Agreeing with Yang et al., (2008), the simulated Gln and Glu spectra using long TE/TM show higher spectral separation than those using short TE/TM at both 3 and 7 T. In addition, long TE/TM also reflects the true Glu/Gln ratio of the phantom more accurately than short TE/TM at both fields. The larger CRLB values of Gln and Glu at long TE/TM, compared to at short TE/TM, are probably caused by their lower spectral SNRs,

## Comparing Gln/Glu Separation Using STEAM with Short and Long TE/TM at 3 and 7 T

---

since the CRLB analysis in LCMoDel is partially reversely linked to spectral SNR (Provencher, 2013).

Based on the similar spectral line-widths represented by FWHM values, all field-specific *in vivo* spectra are considered being acquired under the identical shim condition. With two times the SNR, 7 T *in vivo* spectra using short TE/TM have comparable Glx quantification but significantly different concentrations of Gln and Glu, much smaller CRLBs and less correlation between Gln and Glu, compared to those using long TE/TM. More importantly, the mean level of Glu/Gln ratios in the rPCC region using short TE/TM is more comparable to the literature reported for anterior cingulate cortex region (Stephan et al., 2011; 6.0 vs 4.8) than that using long TE/TM (16.7). The small variance between the ratios at short TE/TM and from the literature is likely because of the regional variations across cingulate cortex (Dou et al., 2013). Analog to the 7 T results, similar Glx concentrations but significantly different Gln and Glu quantification are also found between the 3 T *in vivo* spectra using short and long TE/TM. Considering the similar correlation coefficients between Gln and Glu, significantly different spectral SNRs might be the main reason causing discrepant CRLBs and quantification for Gln and Glu measured with short and long TE/TM. To further explore the importance of SNR in metabolite quantification, PRESS with short TE was applied for Gln and Glu acquisitions at 3 T. The acquired spectra have the highest SNRs in 3 T *in vivo* spectra and their mean Glu/Gln ratio is consistent with literature (Hurd et al., 2004; 3.62 vs 3.65), while the ratio is 2.4 for short TE/TM and 1.0 for long TE/TM.

Higher separation at long TE/TM in *in vitro* spectra and more accurate quantification at short TE/TM in *in vivo* spectra indicate that given sufficient spectral SNR (*in vitro* spectra), the proposed field-specific long TE/TM settings are indeed capable of more accurately separating Gln and Glu than short TE/TM. However, because of more than ten times lower metabolite concentrations and much shorter  $T_2$  relaxation time, *in vivo* spectra cannot be acquired with similar SNRs as *in vitro* spectra, especially using long TE.

## Comparing Gln/Glu Separation Using STEAM with Short and Long TE/TM at 3 and 7 T

---

*In vivo* results demonstrate that the SNRs of spectra using short TE are significantly higher than those using long TE, and accurate metabolite quantifications are respectively obtained from the spectra using short TE in PRESS at 3 T and short TE/TM in STEAM at 7 T. Therefore, high spectral SNR is inferred as the dominant factor for accurate Gln and Glu quantification in *in vivo* spectra.

As reported in the literature (Yang et al., 2008; Stephan et al., 2011), most CRLB values of Glu and Gln using short and long TE/TM are smaller than the values obtained here: 2 vs 4 and 8 vs 7 (Glu), 6 vs 15 and 28 vs 76 (Gln) at 7 T; 8 vs 13 and 10 vs 28 (Glu), 24 vs 31 and 5 vs 27 (Gln) at 3 T. The most probable reason is that for high spectral SNRs, both previous studies measured spectra with more than two times larger voxels and twice the scan averages than this study (8, 9 ml vs 3.75 ml; 256, 288 vs 128). However, in most clinical MRS studies, medical doctors require small voxels to limit partial volume effects and short scan time for patients. Clementi et al., (2005) reported that the increased spectral interference between NAA and Glx are occurred using short TE/TM. However, similar detection of *in vivo* NAA using short and long TE/TM are demonstrated in terms of CRLBs at either 3 T ( $6.8 \pm 2.1$  vs  $6.4 \pm 1.4$ ,  $p = 0.71$ ) or 7 T ( $2.4 \pm 0.5$  vs  $2.0 \pm 0.9$ ,  $p = 0.08$ ).

In addition to STEAM, *in vivo* Gln and Glu were also measured previously using other  $^1\text{H}$ -MRS techniques, such as semi-adiabatic LASER, MEGA-PRESS spectral editing and 2D J-resolved PRESS. Semi-adiabatic LASER sequence with short TE = 24 ms was applied by Öz et al., (2011) for full signal intensity to measure human cerebellum spectra at 4 T. The averaged Glu/Gln ratio is 2.6. MEGA-PRESS with TE = 68 ms was used by Kakeda et al., (2011) to acquire Gln and Glu signals in human parieto-occipital lobe and frontal lobe regions at 3 T. The quantified Glu/Gln ratio is 1.1 with CRLB values 11 and 70 for Gln and Glu. Additionally, 2D J-resolved PRESS was suggested as an effective and stable technique for *in vivo* Gln and Glu acquisitions (Henry et al., 2010). Walter et al., (2009) applied this technique at 3 T to measure Gln and Glu in human pregenual anterior

## Comparing Gln/Glu Separation Using STEAM with Short and Long TE/TM at 3 and 7 T

---

cingulate cortex region. The acquisition time was 16 minutes per voxel and the resulted Glu/Gln ratio is 4.0. Compared to the above-mentioned techniques, STEAM with short TE/TM at 7 T shows the optimal separation for Gln and Glu with high and reasonable Glu/Gln ratio. Furthermore, its much shorter acquisition time, compared to 2D J-resolved PRESS, is particularly suitable for clinical studies.

In conclusion, field-specific long TE/TM proposed by Yang et al., (2008) is indeed able to more accurately separate Gln and Glu than short TE/TM, given sufficient spectral SNR. However, due to the limited spectral SNRs in clinical MRS, the superiority of Gln and Glu separation using long TE/TM is outweighed by the high SNR of short TE/TM acquisition especially at high field. Therefore, STEAM with short TE/TM at 7 T is proposed to be applied in future Gln- and Glu-oriented clinical MRS studies.

Measurement Reproducibility and Systematical Investigations of  
GABA, Gln and Glu Concentrations Using STEAM with Short TE/TM  
at 7 T

---

4

**Measurement Reproducibility and  
Systematical Investigations of GABA, Gln  
and Glu Concentrations Using STEAM with  
Short TE/TM at 7 T**

# Measurement Reproducibility and Systematical Investigations of GABA, Gln and Glu Concentrations Using STEAM with Short TE/TM at 7 T

---

## 4.1 Preface

The main goal in this chapter is to test whether reproducible measurement for *in vivo* glutamine (Gln) and glutamate (Glu) can be achieved at 7 T by applying the stimulated-echo acquisition mode (STEAM) with short echo time (TE) / mixing time (TM; 20 ms / 10 ms) proposed in Chapter 3.

To achieve this goal, four cingulate sub-regions in human brains are systematically measured using STEAM with short TE/TM (20 ms / 10 ms) at 7 T. The corresponding local concentrations of Gln and Glu as well as GABA are obtained, and further corrected for gray matter (GM) content using a newly designed correction method to exclude the potential influence of local GM variations on metabolite concentrations (McLean et al., 2000; Srinivasan et al., 2006). All these concentrations with and without correction are used to quantify the measurement reproducibility.

In addition, all these obtained local metabolite concentrations before and after correction are also used to reveal the regional glutamatergic and GABAergic variations across human cingulate cortex (CC), and compared with their respective receptor densities measured autoradiographically by Palomero-Gallagher et al., (2009), aiming to explore to what extent the local concentrations of the major excitatory neurotransmitter Glu and the major inhibitory neurotransmitter GABA reflect the differences in local Glu and GABA receptor densities and which subtypes of receptors are most strongly represented.

# Measurement Reproducibility and Systematical Investigations of GABA, Gln and Glu Concentrations Using STEAM with Short TE/TM at 7 T

## 4.2 Materials and Methods

### MRS Data Acquisition

Thirty six healthy male subjects ( $27 \pm 3$  years old) were recruited after giving informed written consent in accordance with the approval by the local Institutional Review Board. They were required to stop drinking tea, coffee or smoking at least one hour before the scan sessions. All scan sessions were arranged between 8 A.M. and 8 P.M. with an averaged time difference of 3.8 hours over all subjects.

Ten of these subjects were randomly selected as “retest subjects” and scanned three times within two months in order to evaluate the measurement reproducibility. The remaining twenty six subjects were only scanned one time. Four cingulate sub-regions across CC were measured for spectrum acquisitions, including pregenual anterior CC (pgACC), anterior mid-CC (aMCC) and both rostral and caudal parts of the posterior CC (PCC): rPCC and cPCC (Fig. 4.1).

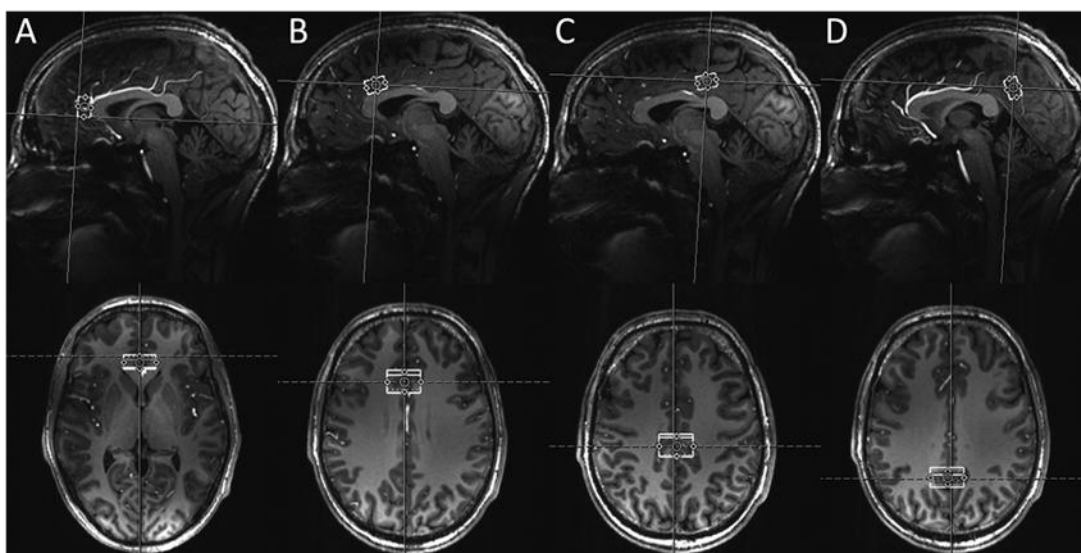


**Figure 4.1** Voxel placement on four ROIs in representative 3D MPRAGE anatomical images: pgACC (A), aMCC (B), rPCC (C) and cPCC (D).

# Measurement Reproducibility and Systematical Investigations of GABA, Gln and Glu Concentrations Using STEAM with Short TE/TM at 7 T

All experiments were performed on a 7 T MR scanner (Siemens MAGNETOM, Erlangen, Germany) using a 24-channel head array coil (Nova Medical, Wilmington, USA). High resolution anatomical images were acquired with the application of the three dimensional (3D) magnetization-prepared rapid gradient echo (MPRAGE) sequences. The corresponding scan parameters were: TE = 2.73 ms, repetition time (TR) = 2300 ms, inversion time (TI) = 1050 ms, flip angle = 5°, bandwidth = 150 Hz/pixel, acquisition matrix = 320 x 320 x 224 and isometric voxel size = (0.8 mm)<sup>3</sup>. A reconstruction procedure was then applied to reconstruct MPRAGE images in the anterior commissure – posterior commissure plane, which provided the anterior – posterior direction for placing MRS voxels. Local B<sub>1</sub> adjustments and local B<sub>0</sub> adjustments were respectively implemented in the voxel-specific regions, in order to achieve optimal local signal-to-noise-ratios (SNRs) and field inhomogeneities. STEAM with variable rate selective excitation (VERSE) pulses were employed for spectrum acquisitions with voxel size of 25 x 15 x 10 mm<sup>3</sup> = 3.75 ml, 128 averages, TR/TE/TM = 3000/20/10 ms, data size = 2048 points and bandwidth = 2800 Hz. Corresponding water reference spectra were also acquired for eddy current correction and metabolite quantification.

The basis set for spectrum analysis was measured using STEAM VERSE with identical TR/TE/TM setting at 7T, which consists of twenty metabolites spectra (acetate, alanine, aspartate, citrate, N-acetylaspartate (NAA), creatine (Cr), GABA, Glu, Gln, glucose, glycine, glycerophosphocholine, glutathione, myo-Inositol, phosphocreatine, lactate, phosphocholine, phosphorylethanolamine, succinate and taurine).

## Data Analysis

LCModel version 6.1.0 (Provencher, 1993) was applied for spectrum analysis. Institutional units (i.u.) were used to express the metabolite concentrations. Standard criteria were applied for selecting spectra with sufficient quality: (i) full width at half maximum (FWHM) of all spectra < 25 Hz, (ii) SNRs of NAA > 8, and (iii) CRLBs of GABA,

# Measurement Reproducibility and Systematical Investigations of GABA, Gln and Glu Concentrations Using STEAM with Short TE/TM at 7 T

Gln and Glu < 20%. The group-wise outliers of region-specific GABA, Gln and Glu concentrations, defined as greater than three times the inter-quartile range, were further detected using Boxplot in SPSS 18 (SPSS for Windows, Chicago III, USA) and excluded.

T<sub>1</sub>-weighted anatomical images of subjects were calculated by means of dividing the MPRAGE images to the gradient echo images measured with TR = 1340 ms, TE = 2.73 ms, flip angle = 5°, bandwidth = 150 Hz/pixel, acquisition matrix = 320 x 320 x 224 and isometric voxel size = (0.8 mm)<sup>3</sup> (van de Moortele et al., 2009), and then segmented into GM, white matter (WM) and cerebrospinal fluid (CSF) intensity maps by applying the unified segmentation option of the SPM 8 software package (Wellcome Trust Center for Neuroimaging, London, United Kingdom). Based on the obtained GM intensity maps, a custom-built program written in MATLAB (The Mathworks, Inc., Natick, MA, USA) was utilized to calculate the GM percentages within respective MRS voxels. Considering the potential influences of local GM content variations on metabolite concentrations, one correction method in Eq.4.1 was designed to correct metabolite concentrations based on the estimated GM contributions for each region individually:

$$MC_{co,i} = MC_{ave} + Res_i \quad [Eq.4.1]$$

For the *i*th subject, the corrected metabolite concentration for each region (MC<sub>co,i</sub>) was calculated by means of the summation of the standardized residual (Res<sub>i</sub>), obtained from a linear regression between uncorrected metabolite concentrations and corresponding GM percentages of the voxels over all regions and subjects, and the mean level (MC<sub>ave</sub>) of the uncorrected metabolite concentrations across all regions and subjects.

## Measurement Reproducibility and Systematical Investigations of GABA, Gln and Glu Concentrations Using STEAM with Short TE/TM at 7 T

---

The reproducibility of GABA, Gln and Glu measurements was assessed using the ten “retest subjects” data in intraclass correlation coefficient (ICC) toolbox of SPSS 18. ICC is able to quantify the measurement reproducibility using coefficients from 0 to 1, in which low values question the reproducibility and a coefficient of 1.0 indicates perfect matches (Weir, 2005). GABA, Gln and Glu concentrations in four regions, after the exclusion of spectra with poor quality and concentration outliers, were not complete for all three scan sessions and all subjects. Random data selections were thus implemented for each subject in three scan sessions to keep complete concentration values for all ten subjects in two scan sessions, with an exception of only seven subjects having at least two valid Gln values in cPCC.

Mean values of the ten retest subjects were calculated and entered into the whole sample. Missing values, due to the removal of spectra with unacceptable quality or concentration outliers, were substituted using the mean levels of the corresponding metabolites in the corresponding regions. In total, ten values (four for GABA and six for Gln) were rejected from the data analysis, corresponding to only a 5% of all entries.

To investigate the difference of GM contents across the four regions, a repeated measures analysis of variance (ANOVA) with the main factor of region and the paired-t tests as post hoc tests were applied in the full data sample. The significant threshold for both tests were set as  $p = 0.05$ . To test the regional variations of local metabolite concentrations across the CC, a separate repeated measures ANOVA with two main effects (metabolite and region) and the interaction effect (metabolite x region) was applied on three metabolite concentrations (GABA, Gln and Glu) in four regions, in which  $p = 0.05$  was also set as the significance threshold. In case that a significant main or interaction effect was found, paired t-tests using bootstrapping (1000 samples) were further used to systematically compare these metabolite concentrations in different regions. Considering the Bonferroni correction for six multiple comparisons,  $p = 0.05/6$

# Measurement Reproducibility and Systematical Investigations of GABA, Gln and Glu Concentrations Using STEAM with Short TE/TM at 7 T

=0.008 was set as the significance threshold. In addition, the metabolite concentration ratios in the four regions were also compared using paired t-tests with bootstrapping.

Lastly, multivariate linear regressions were applied to explore the effect of individual MRS voxel placement, through testing the correlation relationships between metabolite concentrations and normalized voxel positions.

## 4.3 Results

### 4.3.1 Spectrum Quality

All spectra in four regions were measured with high quality: mean SNRs above 30, and mean FWHM values below 10 Hz for all regions except the pgACC region (14.6 Hz). Moreover, the target metabolites (i.e., GABA, Gln and Glu) were quantified with sufficient accuracy: mean CRLB values less than or equal to 10% for GABA, 12% for Gln and 4% for Glu (Fig. 4.2 and Table 4.1).

**Table 4.1** Mean SNR  $\pm$  standard deviation (SD), FWHM  $\pm$  SD and CRLB  $\pm$  SD of GABA, Gln and Glu in pgACC, aMCC, rPCC and cPCC regions across all subjects.

	SNR	FWHM (Hz)	CRLB (%)		
			GABA	Gln	Glu
pgACC	33 $\pm$ 6.8	14.6 $\pm$ 3.1	8.9 $\pm$ 3.3	9.0 $\pm$ 3.3	3.5 $\pm$ 0.9
aMCC	34 $\pm$ 5.9	9.6 $\pm$ 1.6	9.5 $\pm$ 2.0	10.6 $\pm$ 2.3	4.2 $\pm$ 1.9
rPCC	37 $\pm$ 4.5	8.8 $\pm$ 1.4	10.0 $\pm$ 1.8	12.0 $\pm$ 3.1	3.9 $\pm$ 0.9
cPCC	43 $\pm$ 5.8	9.0 $\pm$ 1.6	9.2 $\pm$ 1.7	11.7 $\pm$ 2.1	3.9 $\pm$ 0.8

# Measurement Reproducibility and Systematical Investigations of GABA, Gln and Glu Concentrations Using STEAM with Short TE/TM at 7 T

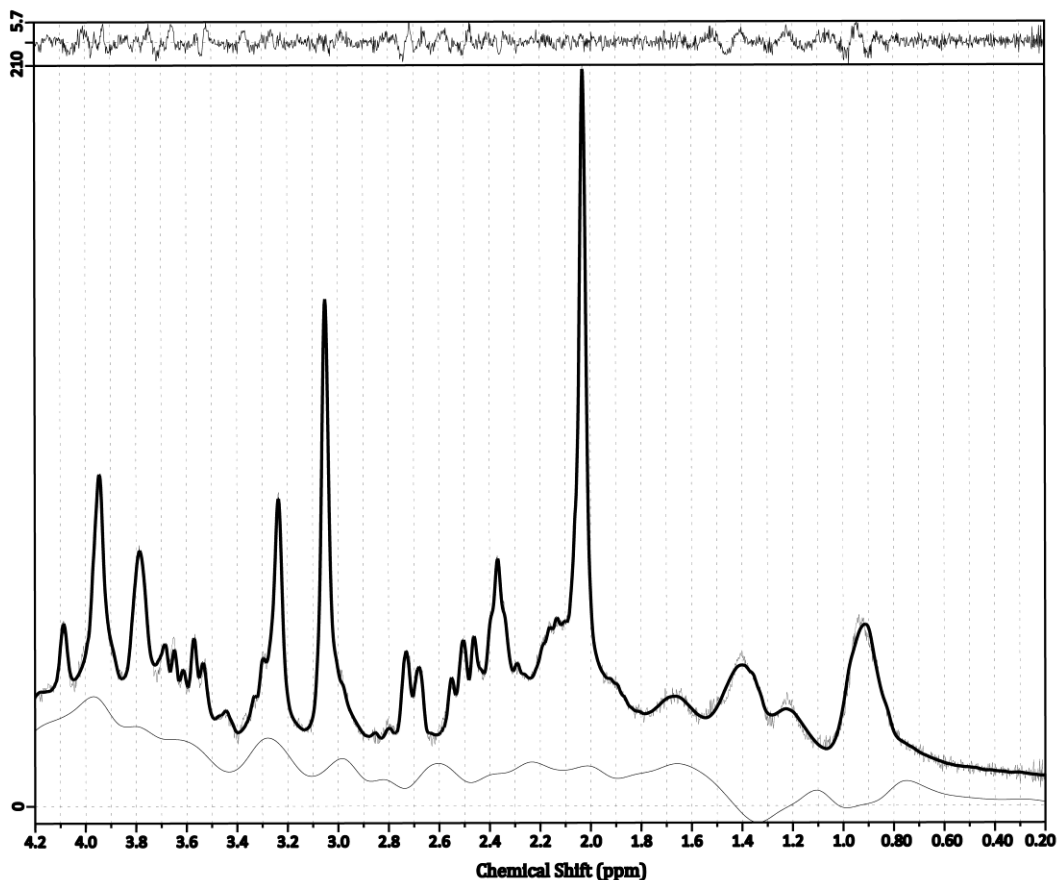
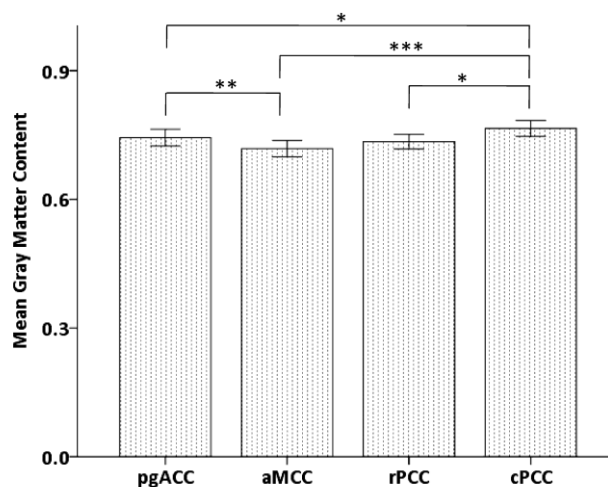


Figure 4.2 An example spectrum in the cPCC region with a flat baseline, SNR 51 and FWHM 6.8 Hz.

## 4.3.2 Regional Variations of Gray Matter across Human Cingulate Cortex

A main effect of region was revealed in the investigation of inter-regional GM variations using repeated measures ANOVA ( $F_{(3,33)} = 8.4, p < 0.001$ ). The post hoc t-tests (Fig. 4.3) showed that the cPCC region had the highest GM contents compared to the remaining three regions (cPCC vs pgACC,  $p = 0.035$ ; cPCC vs aMCC,  $p < 0.001$ ; cPCC vs rPCC,  $p = 0.011$ ), and the GM contents in the pgACC region was significantly higher than those in the aMCC region ( $p = 0.003$ ).

## Measurement Reproducibility and Systematical Investigations of GABA, Gln and Glu Concentrations Using STEAM with Short TE/TM at 7 T



**Figure 4.3** Interregional differences in mean GM content ( $p < 0.001$  is denoted as \*\*\*,  $p < 0.01$  is denoted as \*\*,  $p < 0.05$  is denoted as \*).

### 4.3.3 The Reproducibility of Repeated Measurements

Reproducibility of repeated measurements was confirmed by high ICC values (higher than 0.75) in all cases for all three metabolites. For metabolite concentrations without correction for GM content, comparable ICCs for GABA (.86), Gln (.92) and Glu (.89) across four regions and consistent ICCs for pgACC (.88), aMCC (.89), rPCC (.92) and cPCC (.87) for all metabolites were found. Similarly, the ICCs of corrected metabolite concentrations for GM content (mean .88, Fig. 4.4.B) were unchanged compared to uncorrected metabolite concentrations (mean .89, Fig. 4.4.A).

# Measurement Reproducibility and Systematical Investigations of GABA, Gln and Glu Concentrations Using STEAM with Short TE/TM at 7 T

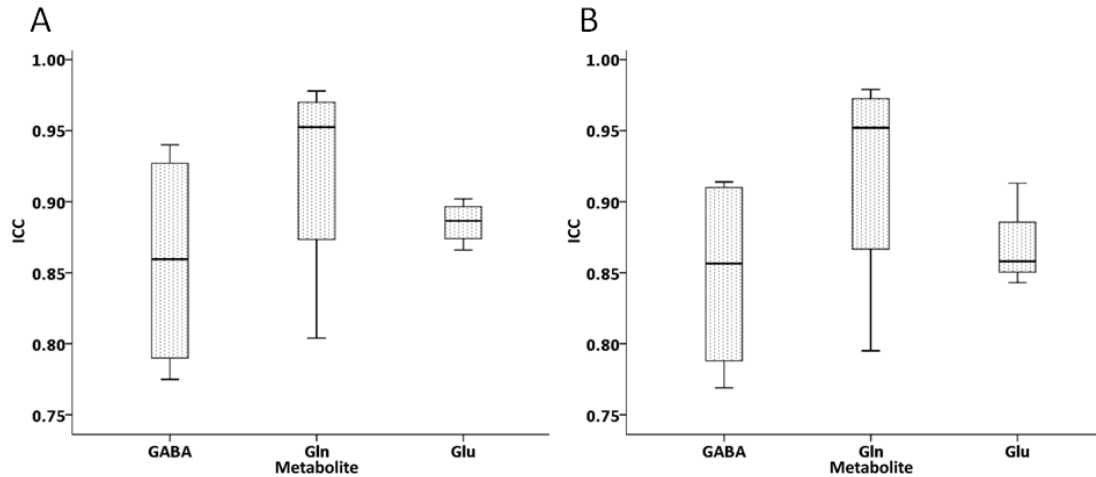


**Figure 4.4** ICCs of the metabolite concentrations (GABA, Gln and Glu) before (A) and after (B) correction for GM content in the pgACC, aMCC and rPCC and cPCC regions.

## 4.3.4 The Regional Variations of GABA, Gln and Glu Concentrations and Ratios in the Cingulate Cortex

For uncorrected metabolite concentrations for GM content, repeated measures ANOVA revealed a significant main effect for region ( $F_{(3,33)} = 7.9, p < 0.001$ ) and also a significant interaction effect (metabolite x region;  $F_{(6,30)} = 4.9, p = 0.001$ ). Further comparisons using paired t-tests with bootstrapping were thus implemented to systematically compare the local metabolite concentrations between all four regions. GABA in the pgACC region had significantly higher concentrations than in the aMCC region ( $T = 3.022, p = 0.002$ ) and rPCC region ( $T = 3.585, p = 0.001$ ), while the increase of GABA concentrations in the pgACC region relative to the cPCC region only survived at uncorrected  $p < 0.05$  level ( $T = 2.218, p = 0.029$ ). Gln in the pgACC region showed the highest concentrations compared to the remaining three regions (pgACC vs aMCC,  $T = 3.161, p = 0.003$ ; pgACC vs rPCC,  $T = 5.406, p = 0.001$ ; pgACC vs cPCC,  $T = 6.156, p =$

## Measurement Reproducibility and Systematical Investigations of GABA, Gln and Glu Concentrations Using STEAM with Short TE/TM at 7 T

---

0.001). Moreover, Gln in the aMCC region had significantly higher concentrations than in the rPCC region ( $T = 2.812, p = 0.006$ ) and also higher concentrations than in the cPCC region ( $T = 2.464, p = 0.020$ ) at uncorrected  $p < 0.05$  level. For Glu, the concentrations in the pgACC region were significantly higher than those in the aMCC region ( $T = 3.332, p = 0.001$ ), significantly higher than those in the rPCC region ( $T = 2.673, p = 0.010$ ) at uncorrected  $p < 0.05$  level, and trend-wisely higher than those in the cPCC region ( $T = 1.617, p = 0.097$ ; Fig. 4.5.A). When metabolite concentrations were corrected for GM content, a significant main effect for region ( $F_{(3,33)} = 9.9, p < 0.001$ ) and a significant interaction effect (metabolite x region;  $F_{(6,30)} = 4.1, p = 0.004$ ) were again revealed using repeated measures ANOVA. Comparison results using paired t-tests kept largely consistent. Only the corrected Gln concentrations in the aMCC region became significantly higher than in the cPCC region (Fig. 4.5.B).

Relative ratios, namely, GABA/Glu for the inhibition/excitation balance and Gln/Glu for the Gln cycling, before and after correction showed comparable comparison results across all four regions. However, the uncorrected GABA/Glu ratios in the pgACC region toward the cPCC region and the uncorrected Gln/Glu ratios in the pgACC region toward the aMCC region varied from trend-wise increases to significant increases at uncorrected  $p < 0.05$  level when they were corrected for GM content. In addition, GABA/Glu ratios before and after correction in the pgACC region toward the aMCC region varied from a trend-wise increase to a significant increase. As a main finding, increased GABA/Glu ratios in the pgACC region compared to the remaining three regions were observed, while a gradual decline in Gln/Glu ratios was found along a rostro-caudal gradient (Fig. 4.6).

# Measurement Reproducibility and Systematical Investigations of GABA, Gln and Glu Concentrations Using STEAM with Short TE/TM at 7 T

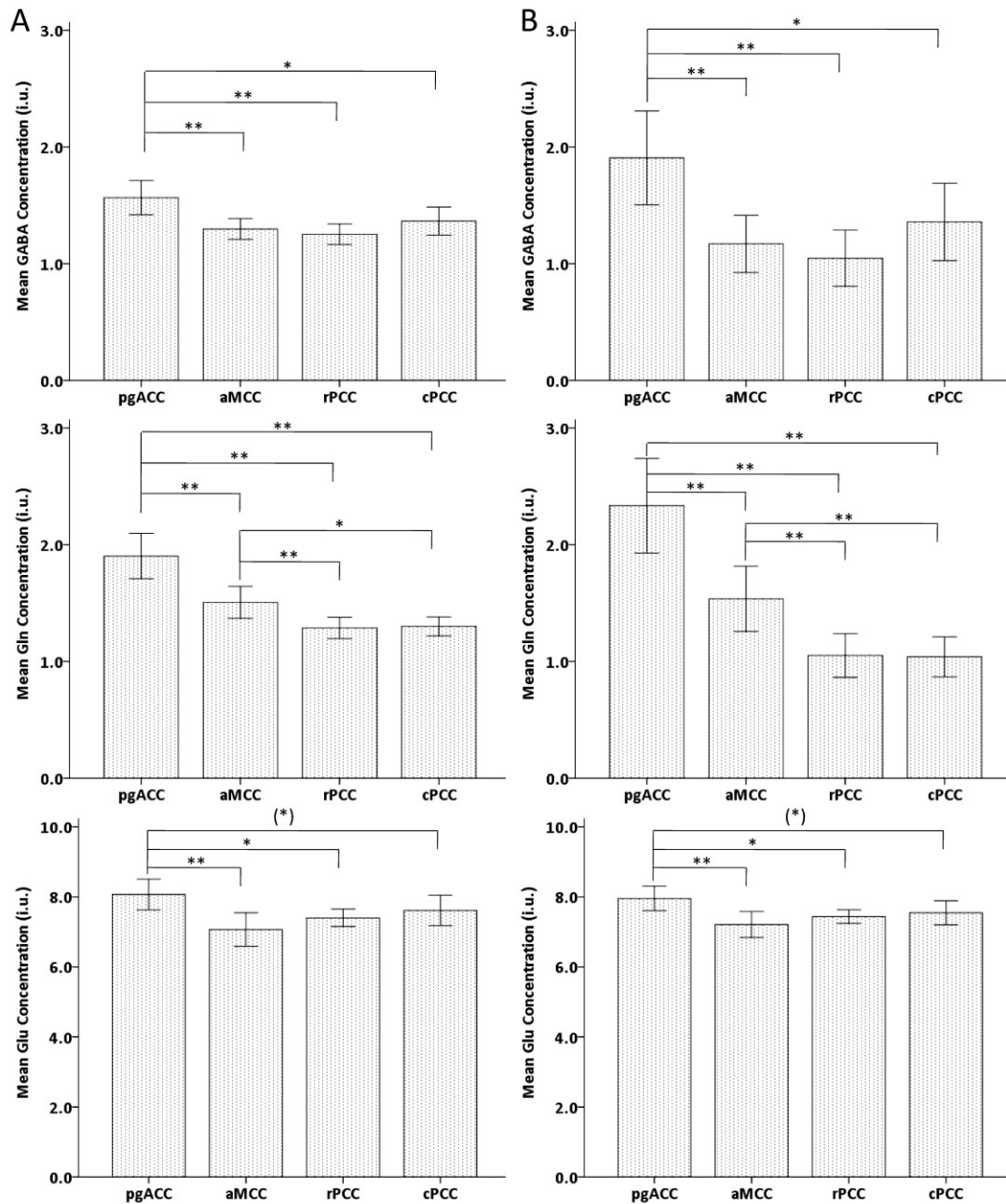


**Figure 4.5** Mean levels of metabolite concentrations of GABA (top), Gln (middle) and Glu (bottom) before (A) and after (B) correction for the GM content in the pgACC, aMCC, rPCC and cPCC regions ( $p < 0.01$  is denoted as \*\*,  $p < 0.05$  is denoted as \* and  $p < 0.1$  is denoted as (\*) ). The metabolite concentrations are expressed in institutional units (i.u.).

# Measurement Reproducibility and Systematical Investigations of GABA, Gln and Glu Concentrations Using STEAM with Short TE/TM at 7 T

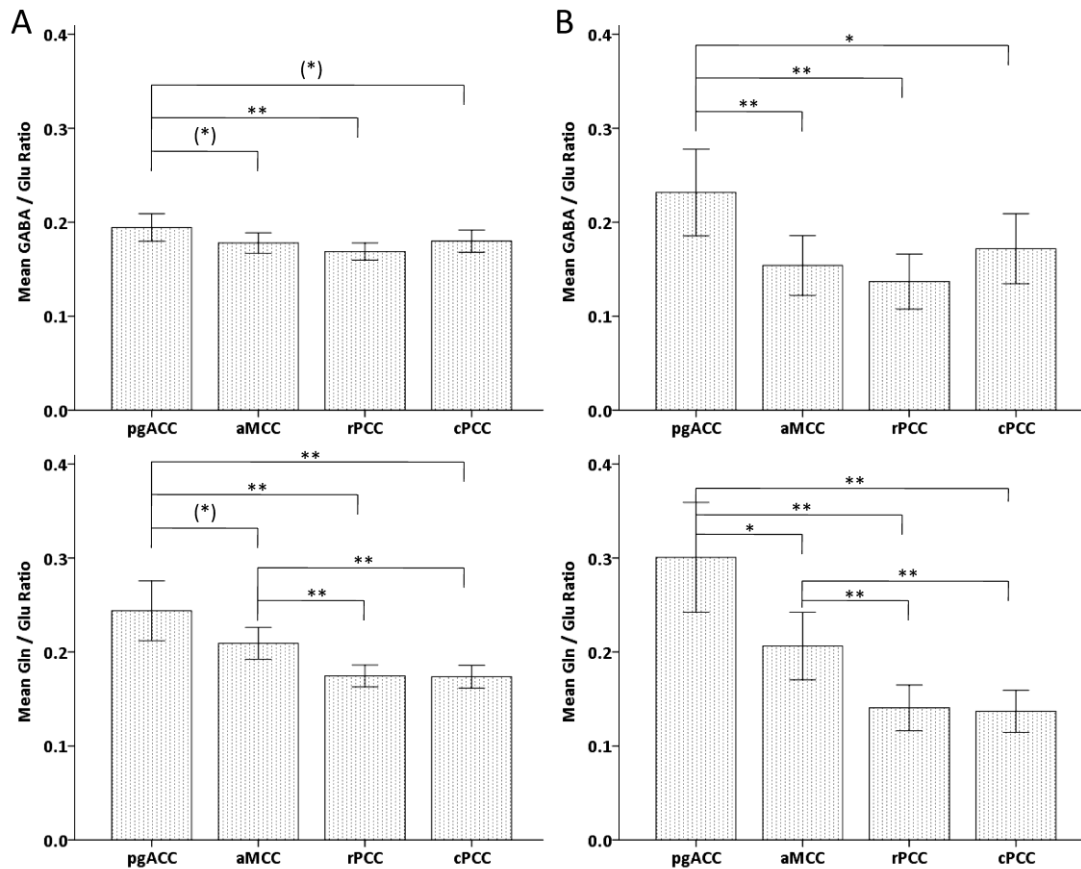


**Figure 4.6** Mean levels of metabolite concentration ratios for inhibition/excitation (GABA/Glu, upper) and indirect Gln cycling (Gln/Glu, lower) by using metabolite concentrations before (A) and after (B) correction for the GM content in the pgACC, aMCC, rPCC and cPCC regions ( $p < 0.01$  is denoted as \*\*,  $p < 0.05$  is denoted as \* and  $p < 0.1$  is denoted as (\*) ).

## 4.3.5 The Effects of the Voxel Placement Deviations on Metabolite Concentrations

No major effects of regional voxel positions were revealed on metabolite concentrations using multivariate linear regressions.

# Measurement Reproducibility and Systematical Investigations of GABA, Gln and Glu Concentrations Using STEAM with Short TE/TM at 7 T

---

## 4.4 Discussion

In this chapter, STEAM with short TE/TM (20 ms / 10 ms) proposed for optimal Gln and Glu acquisitions and separation in Chapter 3 was applied at 7 T to systematically measure Gln and Glu as well as GABA signals in four sub-regions across human CC. The corresponding local metabolite concentrations were obtained and corrected for excluding the potential effects of GM content variations across the CC. Partial local metabolites concentrations, acquired in the test-retest measurements, were used to assess the measurement reproducibility, and the whole sample data were analyzed to reveal for the first time the intra-subject regional variations of metabolite concentrations across the CC.

Applying standard spectral quality criteria, 95% metabolites are proven to be successfully measured. Besides the results shown in Chapter 3, the high success rate of metabolite acquisitions obtained here can again demonstrate the reliable Gln and Glu detection using STEAM with short TE/TM. In addition, the reported concentration ratios of GABA, Gln and Glu relative to Cr in the pgACC region (Walter et al., 2009) are also comparable to the values shown in this study: Gln/Cr (0.34 vs 0.35), Glu/Cr (1.35 vs 1.47) and GABA/Cr (0.21 vs 0.29).

As a significant variation of GM contents was found across the CC, the correction of metabolite concentrations for voxel compositions should be taken into account. Since there is currently no gold-standard method allowing the metabolite concentration correction for tissue compositions, one method using linear regression is designed in this study to correct metabolite concentrations for GM contents based on the estimates of the influence of GM variations. The effects of WM and CSF on metabolite concentrations are not considered here, since metabolites are found having much lower concentrations in WM and CSF (McLean et al., 2000; Srinivasan et al., 2006; Stephenson

## Measurement Reproducibility and Systematical Investigations of GABA, Gln and Glu Concentrations Using STEAM with Short TE/TM at 7 T

---

et al., 2011; Lynch et al., 1993; Mandal., 2007) and the mean percentage of CSF to the whole voxel content is no higher than 5% in this study.

Measurement reproducibility is confirmed using test-retest data with and without correction for GM content. The corresponding high ICC values ( $> 0.75$ , the normal threshold value for good reproducibility; Lockhart et al., 2008) demonstrate a high reproducibility of Gln, Glu and GABA measurements using STEAM with short TE/TM. Although merely the spectra fulfilled the quality criteria are applied in the ICC analysis, only 2 of 120 spectra are excluded from the test-retest dataset. Moreover, the accurate and reproducible measurements for GABA indicate that STEAM with short TE/TM at 7 T can not only be applied for reliable detection of Gln and Glu but also be used for measuring those metabolites with small signals (e.g., GABA; Northoff et al., 2007).

The local metabolite concentrations and concentration ratios indeed co-vary with known receptor distributions along anatomically defined sub-regions across CC. A previous study reported a gradual decline of AMPA receptors from above-average densities in the pgACC region towards average levels in the aMCC region, and further caudally sub-average densities in the regions around the central sulcus (Palomero-Gallagher et al., 2009). As an NMDA receptor antagonist, the relevant antidepressant action of ketamine is mainly mediated via activation/translocation of AMPA receptors, which is similar to other glutamate modulating agents (e.g., riluvole or lamotrigine; Du et al., 2006). The suggestion supports the reported treatment effects in the pgACC region, agreed with increased Gln cycling and predicted by local Gln concentrations (Salvadore et al., 2012). This is still an indirect link and however needs to be considered as the first evidence connecting the local metabolite concentration and a receptor subtype density that is referred to increased metabolite levels in pharmacology and Gln cycling.

## Measurement Reproducibility and Systematical Investigations of GABA, Gln and Glu Concentrations Using STEAM with Short TE/TM at 7 T

---

On the other hand, the study regarding the link between GABA concentrations and their relevance for actual synaptic GABAergic activity in humans has not been established yet. The here found highest GABA concentrations in the pgACC region reflect the higher GABA<sub>B</sub> receptor densities compared with other three cingulate compartments (Palomero-Gallagher et al., 2009). Oppositely, the local GABA concentrations correlate inversely with GABA<sub>A</sub> receptor densities, since GABA<sub>A</sub> receptor shows the lowest concentrations in the pgACC region across all four cingulate sub-regions (Palomero-Gallagher et al., 2009). Therefore, GABA release in the pgACC region would mainly result in slow synaptic inhibition via GABA<sub>B</sub> receptors, whereas the mid-CC (MCC) region and the PCC region would be subject to the fast component of GABAergic inhibition mediated to a greater extent by GABA<sub>A</sub> receptors. Interestingly, activation of presynaptic GABA<sub>B</sub> receptors suppresses multi-vesicular release and thus decreases synaptic Glu concentration (Chalifoux and Carter, 2010). This would be able to explain why the pgACC region has the highest GABA/Glu ratios. This characteristic ratio, together with its receptor fingerprints, would indicate that the pgACC region is subject to a higher degree of inhibition compared with the MCC or PCC region. Northoff et al., (2007) indeed reported that regional GABA concentrations are correlated with the amount of negative blood oxygen-level-dependent responses in the pgACC region across subjects, it should however be aware that a similar effect of covariance of markers of an inhibition/excitation balance and the known regional baseline mechanisms of task induced activations and deactivations are found here.

The distinction of anatomical boundaries in the PCC region is a critical limitation in this study. Partitions adjacent to each other in this region are relatively small and have opposing receptor densities. Using the current voxel size defined in this study, it is difficult to measure individual partition without partial volume effect. Therefore, more careful comparisons between the local profiles of metabolite concentrations and the receptor fingerprints in the posterior voxels would be expected to find out more

## Measurement Reproducibility and Systematical Investigations of GABA, Gln and Glu Concentrations Using STEAM with Short TE/TM at 7 T

---

variations between the posterior voxels. In addition, PCC region is also expected to have higher GABA/Glu and Glu/Gln ratios, if the voxel position is more ventral and caudal, towards the retrosplenial – precuneus portion. However, the actual cPCC voxel is located quite dorsally and not overlapped with the posterior default mode network in the PCC region (Yu et al., 2011).

In summary, the study has demonstrated that the application of STEAM with short TE/TM at 7 T, which was proposed in the previous chapter, can measure Gln and Glu with high reproducibility and also acquire GABA with high reliability. In addition, the distributions of local GABA, Gln and Glu concentrations across the CC are for the first time revealed and indeed co-varied with the fingerprints of previously reported receptors.

# 5

## **Automatic Voxel Positioning for MR Spectroscopy at 7 T**

## 5.1 Preface

This chapter aims to test whether spectroscopy voxels can be automatically prescribed with high accuracy and reproducibility in high field longitudinal magnetic resonance spectroscopy (MRS) studies.

MRS voxels in longitudinal MRS studies are usually positioned manually by physicians or well trained technicians using visual determinations (Houkin et al., 1993; Schott et al., 2010). Due to the required identical voxel localizations, manual voxel prescription needs additional time, i.e., up to several minutes per voxel, to carefully adjust the localizations and orientations of voxels at each scan session (Itti et al., 2001, Benner et al., 2006). In addition, manual voxel prescription can usually introduce variability of voxel positions at multiple scan sessions because of the varied brain positions of subjects at different scan sessions or the variability of intra- and inter-operators (Itti et al., 2001; Chen et al., 2011). The extra scan time is a problem for patient measurements, and the voxel displacements between different scan sessions may allow for erroneous estimations for the local concentrations of metabolites. Therefore, for efficient and reliable voxel positioning in longitudinal MRS studies, automatic voxel prescription is greatly desired.

Many automatic scan prescription methods have been previously proposed and applied in magnetic resonance (MR) image studies at field strengths up to 3 T. They are geometrical landmarks based method (Itti et al., 2001), image alignment using spherical navigator echoes (Welch et al., 2002; 2004), image based registration algorithm using cross-correlation of the localizer images (Gedat et al., 2004), image based auto-alignment method using statistical atlas (Van der Kouwe et al., 2005), combination of feature landmarks and image registration (Sharp et al., 2005) and imaging registration with an active shape mode (Zhang et al., 2009). However, due to the potential interference between automatic position detection and high field inhomogeneity (e.g., 7 T) and precise positioning requirement for small MRS voxels, no automatic voxel positioning technique has been applied in high field longitudinal MRS studies so far.

# Automatic Voxel Positioning for MR Spectroscopy at 7 T

---

In this chapter, a vendor-provided automatic voxel positioning (Auto-Align) technique is tested for the first time to prescribe MRS voxels in a 7 T longitudinal MRS study. The accuracy and reproducibility of automatic voxel prescription are systematically estimated and further compared to manual voxel prescription.

## 5.2 Materials and Methods

### Data Acquisition

Twenty four healthy subjects were enrolled in this study after a standard clinical interview for excluding history and present psychiatric or neurological illnesses and self-report questionnaires approved by the local Institutional Review Board. Twelve ( $28 \pm 7$  years old) of them were randomly chosen to apply automatic MRS voxel prescription at three separate scan sessions. In comparison, the remaining twelve ( $30 \pm 4$  years old) attended three scan sessions but measured with manual voxel prescription for MRS voxel placement.

All experiments were implemented on a 7 T MR scanner (Siemens MAGNETOM, Erlangen, Germany). 32-channel head array coil (Nova Medical, Wilmington, USA) was applied in the experiments using automatic voxel prescription. The Siemens-provided landmark based pre-scan sequence was initially applied at each scan session. The corresponding scan parameters included: echo time (TE) = 1.53 ms, repetition time (TR) = 4 ms, flip angle (FA) =  $16^\circ$ , bandwidth (BW) = 550 Hz/Px, acquisition matrix = 160 x 160 x 128 and isometric voxel size =  $(1.6 \text{ mm})^3$ . It took 17 s scan time to run this sequence and an additional 26 s for on-line image co-registration under the Siemens image reconstruction hardware of Intel(R) Xeon(R) with 2.8 GHz CPU and 32 GB RAM (Fig. 5.1). All subsequent imaging volumes, e.g.,  $T_1$ -weighted anatomical images and spectroscopy voxels, were defined manually at the first scan session and prescribed automatically in the following two scan sessions. A three dimensional (3D) magnetization-prepared rapid gradient echo (MPRAGE) sequence (TE = 2.73 ms, TR = 2300 ms, inversion time (TI) =

## Automatic Voxel Positioning for MR Spectroscopy at 7 T

---

1050 ms, FA = 5°, BW = 150 Hz/Px, acquisition matrix = 320 x 320 x 224 and isometric voxel size = (0.8 mm)<sup>3</sup>) was used to acquire high resolution anatomical images. The acquisition time was six minutes and one second. All acquired MPRAGE images were then reconstructed into the anterior commissure – posterior commissure plane, which provided the anterior – posterior direction for placing MRS voxels in two cingulate sub-regions: pregenual anterior cingulate cortex (pgACC) and anterior mid-cingulate cortex (aMCC; Fig. 5.2). After local B<sub>1</sub> and local B<sub>0</sub> adjustments, optimal signal-to-noise-ratio (SNR) and field homogeneity were respectively achieved within the voxel-specific regions. Stimulated echo acquisition mode (STEAM) with variable rate selective excitation (VERSE) pulses were then applied to acquire spectra with 128 averages, TR/TE/ mixing time (TM) = 3000/20/10 ms, voxel size = 20 x 15 x 10 mm<sup>3</sup> = 3 ml for the pgACC region and 25 x 15 x 10 mm<sup>3</sup> = 3.75 ml for the aMCC region, data size = 2048 points and BW = 2800 Hz. Each region was measured with six minutes and thirty six seconds scan time. Corresponding water reference spectra were also acquired for eddy current correction and metabolite quantification.

24-channel head array coil (Nova Medical, Wilmington, USA) was applied in the experiments with manual voxel prescription. Based on the 0.8 mm resolution isotropic 3D MPRAGE images reconstructed in the above-mentioned procedure, MRS voxels with voxel size 25 x 15 x 10 mm<sup>3</sup> = 3.75 ml were manually prescribed in the pgACC and aMCC regions by a specially trained technician at all three scan sessions. Following the voxel positions defined at the first scan session, the technician took up to two minutes for each voxel prescription in the following two scan sessions. After the voxel-wise optimization using local B<sub>1</sub> and B<sub>0</sub> adjustments, the above mentioned STEAM with VERSE pulses were applied for spectrum acquisitions, with an exception that two of twelve subjects were measured using TM = 15 ms instead of 10 ms. Corresponding water reference spectra for eddy current correction and metabolite quantification were acquired.

## Automatic Voxel Positioning for MR Spectroscopy at 7 T

A sequence-specific *in vitro* basis set measured with TR/TE/TM (3000 ms / 20 ms / 10 ms) at 7 T was applied for *in vivo* spectrum analysis. This basis set includes eighteen major metabolite spectra (alanine, aspartate, citrate, N-acetylaspartate (NAA), N-Acetylaspartylglutamic acid, creatine, GABA, glutamate, glutamine, glucose, glycerophosphocholine, glutathione, myo-Inositol, phosphocreatine, phosphocholine, phosphorylethanolamine, succinate and taurine).

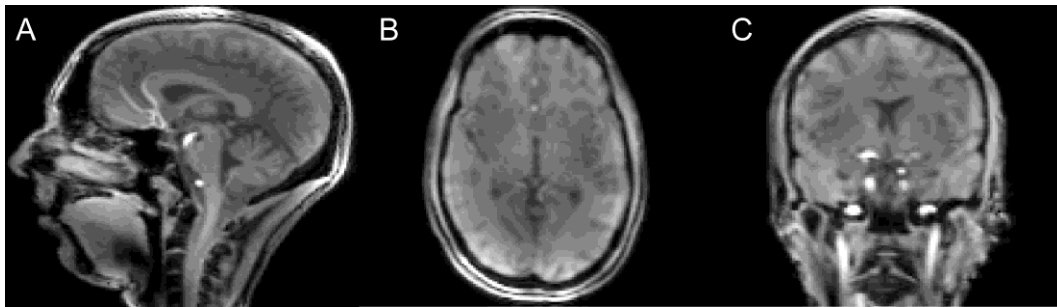


**Figure 5.1** Representative vendor-provided pre-scan images after on-line co-registration (A, sagittal view; B, transverse view; C, coronal view).

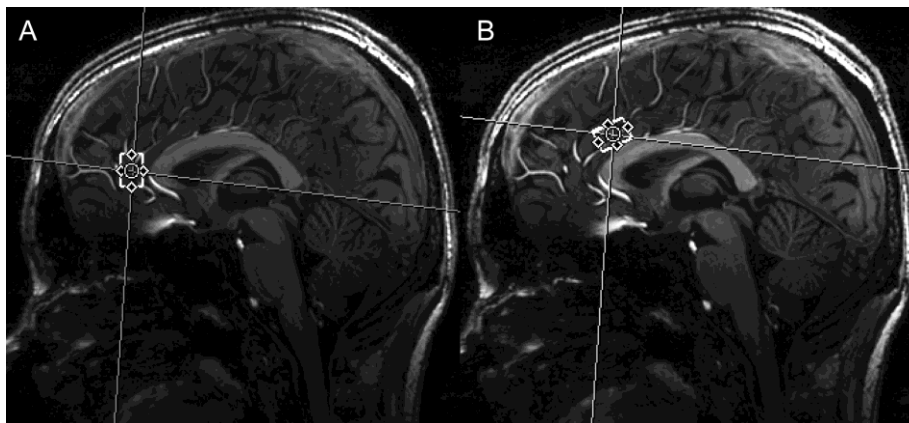


**Figure 5.2** Representative voxel placement in the pgACC (A) and aMCC (B) regions in 3D MPRAGE anatomical images.

### Data Analysis

Binary masks of MRS voxels, which were MPRAGE image based, were created by a custom-built program written in MATLAB (MathWorks). Using the co-registration option

## Automatic Voxel Positioning for MR Spectroscopy at 7 T

---

in SPM 8 (Wellcome Trust Center for Neuroimaging, London, United Kingdom; Ashburner et al., 2013), the MPRAGE images from the second and third scan sessions, together with the corresponding binary voxels, were co-registered into the MPRAGE images from the first scan session. All co-registered voxel binary masks as well as the binary masks from the first scan session were calculated using the image calculation option of the SPM 8. The geometric overlap ratios of the voxels from the second and third scan sessions relative to the first scan session were thus obtained respectively.

The built-in paired t-test toolbox in SPSS 18 (SPSS for Windows, Chicago III, USA) was applied to statistically estimate the reproducibility of automatic and manual voxel prescription. With the significance threshold  $p = 0.05$ , paired t-tests directly compared the region-specific voxel overlap ratios between the first and second scan sessions (sessions 1 and 2) with those between the first and third scan sessions (sessions 1 and 3).

Excluding the spectra of two subjects measured with  $T_M = 15$  ms, the remaining spectra of twenty two subjects were analyzed using LCModel version 6.3.0 (Provencher, 1993; Provencher, 2013). As the output results, the spectral SNRs, Cramer-Rao lower bound (CRLB) values (Cavassila et al., 2001) and the concentrations of metabolites were obtained. The metabolite concentrations were expressed with institutional units (i.u.). To exclude spectra with insufficient quality, strict criteria were applied: (i) spectral SNRs  $< 8$ , and (ii) CRLB values of NAA, creatine + phosphocreatine (Cr) and glutamate + glutamine (Glx)  $> 10\%$ . Because of the strongest signals across all metabolites, NAA, Cr and Glx were chosen as representative metabolites to estimate spectrum quality. The group-wise outliers of region-specific NAA, Cr and Glx concentrations were respectively detected using Boxplot toolbox in SPSS 18, which were defined as greater than three times the inter-quartile range. Total seven concentration values of four spectra were removed from the whole 396 entries.

## Automatic Voxel Positioning for MR Spectroscopy at 7 T

---

Local concentrations of metabolites NAA, Cr and Glx in three scan sessions were used to calculate the coefficients of variation (CV) which was defined as standard deviations (SDs) / mean values, in order to assess the reproducibility of spectrum detection across three scan sessions with automatic and manual voxel prescription.

### 5.3 Results

Over all three scan sessions and two brain regions across all subjects, the mean voxel geometric overlap ratio  $\pm$  SD was  $0.91 \pm 0.06$  for automatic voxel prescription and  $0.70 \pm 0.14$  for manual voxel prescription (Fig. 5.3 and 5.4).

Using paired t-tests, region-specific voxel overlap ratios between sessions 1 and 2 and between sessions 1 and 3 were directly compared. For voxels using automatic voxel prescription, comparable voxel overlap ratios were found in both the pgACC region ( $T = 0.17$ ,  $p = 0.87$ ) and aMCC region ( $T = 0.10$ ,  $p = 0.92$ ; mean:  $0.92 \pm 0.06$  vs  $0.91 \pm 0.05$  for pgACC;  $0.91 \pm 0.06$  vs  $0.91 \pm 0.07$  for aMCC). In contrast, for voxels with manual voxel prescription, voxel overlap ratios between sessions 1 and 2 were found significantly higher than those between sessions 1 and 3 in both the pgACC region ( $T = 4.52$ ,  $p = 0.001$ ; mean:  $0.82 \pm 0.08$  vs  $0.60 \pm 0.14$ ) and aMCC region ( $T = 2.47$ ,  $p = 0.031$ ; mean:  $0.73 \pm 0.07$  vs  $0.65 \pm 0.14$ ).

All spectra were measured with sufficient quality: the mean SNRs  $> 30$ ; the CRLBs of NAA  $< 3\%$ , of Cr  $< 3\%$  and of Glx  $< 5\%$  (Table 5.1, Fig. 5.5). Additionally, the mean levels of local NAA, Cr and Glx across all sessions and subjects and the averaged CVs of their concentrations across all subjects are shown in Tables 5.2 and 5.3. Compared to manual voxel prescription, automatic voxel prescription allows the metabolite concentrations to have lower CVs in both the pgACC and aMCC regions (mean:  $5.3\%$  vs  $11.2\%$  for pgACC;  $5.0\%$  vs  $13.7\%$  for aMCC; Table 5.3).

## Automatic Voxel Positioning for MR Spectroscopy at 7 T

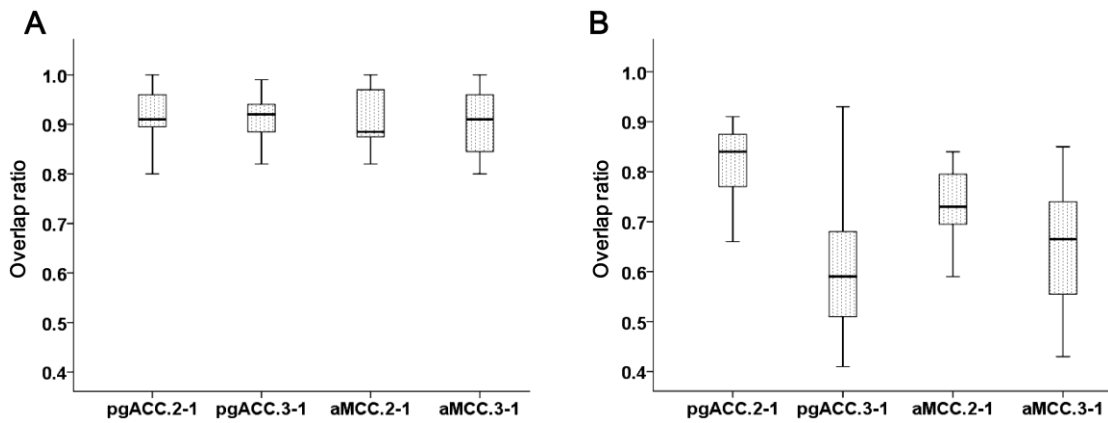


**Figure 5.3** The geometric overlap ratios of MRS voxels prescribed at the second to the first scan sessions (denoted as “2-1”), and at the third to the first scan sessions (denoted as “3-1”) using automatic voxel prescription (A) and manual voxel prescription (B) for both pgACC and aMCC regions across all subjects.

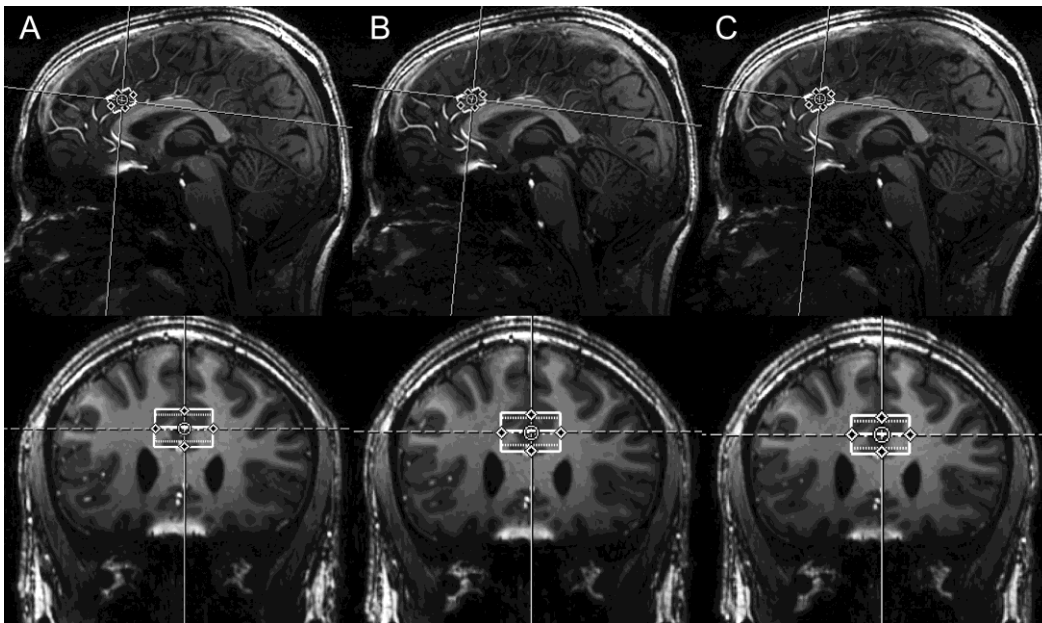


**Figure 5.4** An example within-subject MRS voxel prescriptions in the aMCC region using automatic voxel prescription by the vendor-provided automatic voxel positioning technique. Based on 3D MPRAGE anatomical images, the voxels were manually defined at the first scan session (A) and automatically prescribed at the second and third scan sessions (B, C). No noticeable variations of voxel locations are found.

## Automatic Voxel Positioning for MR Spectroscopy at 7 T

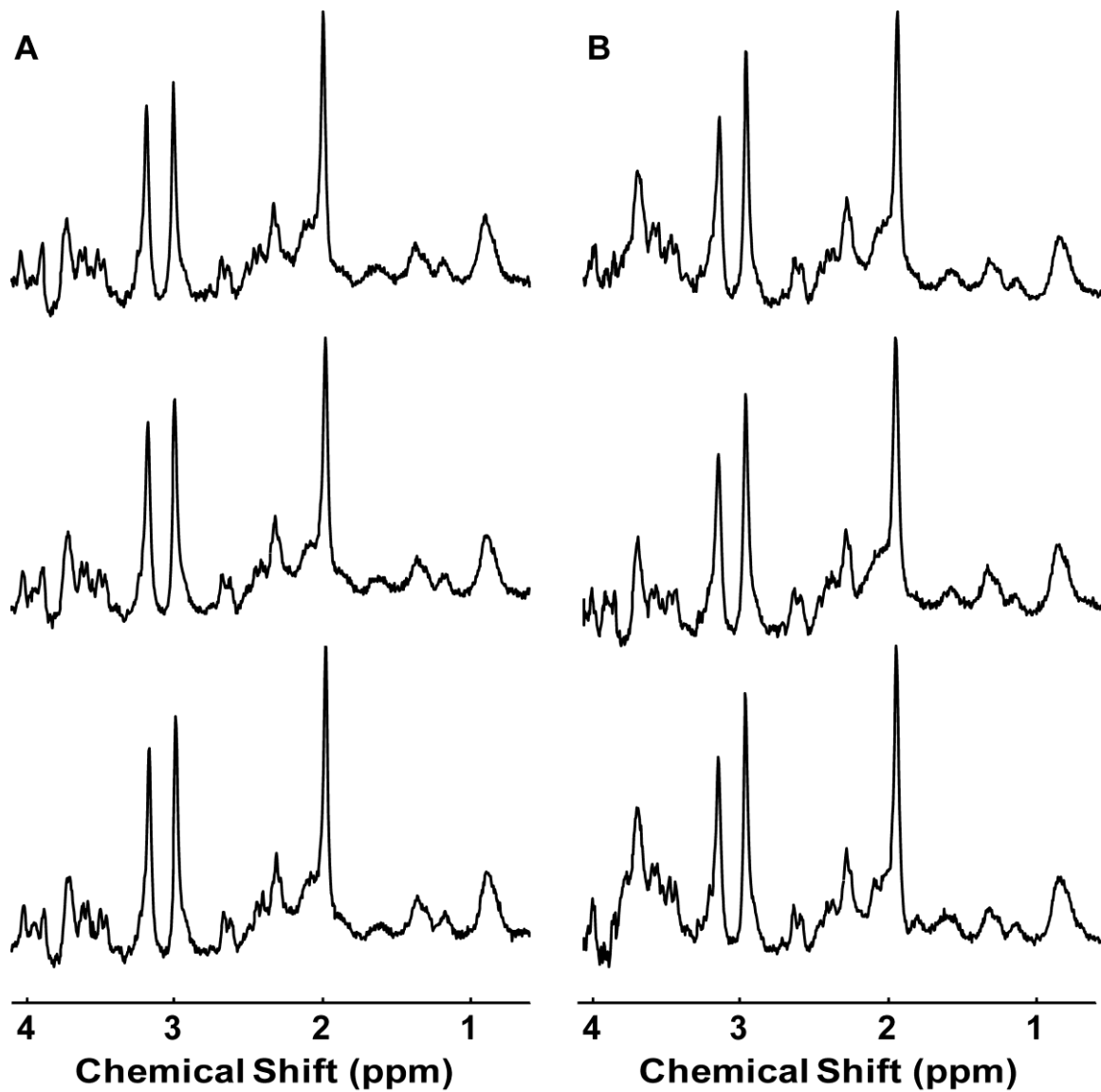


**Figure 5.5** Example within-subject MRS spectra of the pgACC region measured using automatic (A) and manual voxel prescription (B) at the first scan session (upper), at the second scan session (middle) and at the third scan session (bottom).

## Automatic Voxel Positioning for MR Spectroscopy at 7 T

**Table 5.1** Spectra in the pgACC and aMCC regions were measured at three scan sessions using automatic and manual voxel prescription. The corresponding mean SNRs  $\pm$  SDs and CRLBs  $\pm$  SDs of NAA, Cr and Glx are shown.

Type	Region	Session	SNR	CRLB (%)		
				NAA	Cr	Glx
Automatic Voxel Prescription	pgACC	1	46 $\pm$ 6	2.4 $\pm$ 1.7	1.7 $\pm$ 0.5	3.3 $\pm$ 0.6
		2	47 $\pm$ 5	2.0 $\pm$ 0.9	1.7 $\pm$ 0.5	3.2 $\pm$ 0.4
		3	46 $\pm$ 7	1.5 $\pm$ 0.7	1.5 $\pm$ 0.5	3.2 $\pm$ 0.4
	aMCC	1	42 $\pm$ 10	1.7 $\pm$ 0.7	1.4 $\pm$ 0.5	3.8 $\pm$ 0.9
		2	43 $\pm$ 11	1.6 $\pm$ 0.6	1.3 $\pm$ 0.4	3.5 $\pm$ 0.7
		3	46 $\pm$ 4	1.8 $\pm$ 0.4	1.4 $\pm$ 0.5	3.5 $\pm$ 0.5
Manual Voxel Prescription	pgACC	1	35 $\pm$ 7	2.7 $\pm$ 1.4	2.7 $\pm$ 1.1	4.1 $\pm$ 1.4
		2	36 $\pm$ 9	2.4 $\pm$ 1.4	2.5 $\pm$ 0.8	4.2 $\pm$ 0.9
		3	37 $\pm$ 8	2.4 $\pm$ 1.0	2.1 $\pm$ 0.7	3.9 $\pm$ 1.1
	aMCC	1	37 $\pm$ 4	2.1 $\pm$ 0.3	1.9 $\pm$ 0.3	3.5 $\pm$ 0.7
		2	38 $\pm$ 5	2.4 $\pm$ 0.5	1.9 $\pm$ 0.3	3.4 $\pm$ 0.7
		3	33 $\pm$ 7	2.1 $\pm$ 0.6	1.6 $\pm$ 0.5	3.7 $\pm$ 0.9

**Table 5.2** Spectra were acquired in human pgACC and aMCC regions with automatic and manual voxel prescription at three different scan sessions. The corresponding mean metabolite concentrations  $\pm$  SDs of local NAA, Cr, and Glx are displayed. The metabolite concentrations are expressed in institutional units (i.u.).

Type	pgACC			aMCC		
	NAA	Cr	Glx	NAA	Cr	Glx
Automatic	8.6 $\pm$ 0.6	9.1 $\pm$ 0.5	7.9 $\pm$ 0.6	8.9 $\pm$ 0.7	9.4 $\pm$ 0.4	7.4 $\pm$ 0.3
Manual	9.2 $\pm$ 1.1	9.5 $\pm$ 1.0	7.4 $\pm$ 0.5	10.0 $\pm$ 1.1	10.1 $\pm$ 1.0	7.6 $\pm$ 1.2

## Automatic Voxel Positioning for MR Spectroscopy at 7 T

**Table 5.3** Mean CVs (%)  $\pm$  SDs of local NAA, Cr and Glx concentrations across all subjects are shown.

Type	pgACC			aMCC		
	NAA	Cr	Glx	NAA	Cr	Glx
Automatic	6.2 $\pm$ 4.6	4.0 $\pm$ 2.8	5.7 $\pm$ 6.0	6.4 $\pm$ 6.3	3.1 $\pm$ 2.2	5.5 $\pm$ 1.7
Manual	11.7 $\pm$ 6.9	9.5 $\pm$ 3.6	12.5 $\pm$ 11.5	11.8 $\pm$ 10.2	12.9 $\pm$ 10.4	16.3 $\pm$ 15.1

### 5.4 Discussion

In this chapter, MRS voxels were for the first time prescribed automatically in a 7 T longitudinal MRS study, using a vendor-provided automatic voxel positioning technique. Through prescribing MRS voxels in two sub-cingulate regions of healthy subjects at three scan sessions, the accuracy and reproducibility of automatic voxel prescription were systematically estimated and further compared to manual voxel prescription.

Automatic voxel prescription demonstrates in this study that highly accurate and reproducible voxel prescription can be achieved at multiple high field MRS scan sessions with its application, even though high field inhomogeneity can potentially interfere with automatic position detection and small MRS voxels require highly precise positioning. Relative to 70% voxel overlap of manual voxel prescription, 91% voxel overlap proves the accuracy of automatic voxel prescription. Additionally, comparable voxel prescriptions across different scan sessions confirm the high reproducibility of automatic voxel prescription. In comparison, using manual voxel prescription, voxel overlap ratios between sessions 1 and 2 are significantly higher than those between sessions 1 and 3. It indicates that the manual voxel prescription at multiple scan sessions is not as reproducible as automatic voxel prescription, and the corresponding introduced deviations of voxel locations are getting larger as the scan session is farther from the first scan session.

## Automatic Voxel Positioning for MR Spectroscopy at 7 T

---

Evaluating by strict spectral quality criteria, 98% spectra are validated to be successfully measured in the voxels prescribed with automatic and manual voxel prescription. Since the local metabolite concentrations with automatic voxel prescription have much lower CVs than those with manual voxel prescription, it can be inferred that the larger deviations of voxel placement introduced by manual voxel prescription may be the reason resulting in the detection of the local metabolites with more variations. This increased concentration variability can potentially allow for erroneous estimation for local metabolites in longitudinal studies.

Previously, other automatic image prescription techniques have been applied in clinical longitudinal MR image studies at 1.5 T, e.g., tracking lesions in multiple sclerosis and symptoms in neurodegenerative disorders (Molyneux et al., 1998; Freeborough et al., 1996). Highly accurate and reproducible positioning was also reported. As an example, Benner et al., (2006) applied both the manual slice prescription and an image based automatic alignment technique (Van der Kouwe et al., 2005) to prescribe MR images in patients' brains at multiple scan sessions, respectively. The automatically aligned images showed less variation between different scan sessions, compared to the images using manual slice prescription.

However, no application of automatic voxel prescription has been, to our knowledge, established in high field MRS studies so far. Besides the above-mentioned high accuracy and reproducibility, the vendor-provided automatic voxel positioning technique is fully automated for voxel volume positioning in the follow-up scan sessions after the determination of voxel positions at the first session. In addition, compared to the required several minutes for manual voxel placement, this vendor-provided technique requires only 43 s per scan session. The shortened scan time is thus able to be used to optimize MRS acquisitions, e.g., optimizing voxel shimming. Therefore, automatic instead of manual voxel prescription is indeed an effective and efficient solution to prescribe MRS voxels at multiple scan sessions.

## Automatic Voxel Positioning for MR Spectroscopy at 7 T

---

The potential head motion which was not taken into account during the scans is one limitation of this study. The brain motion between the initial pre-scan and MPRAGE image acquisitions can to some degree cause inaccurate image prescriptions. The brain motion between MPRAGE and spectrum acquisitions can influence the detection of local metabolite spectra. Therefore, to control for the potential head motion, motion correction techniques, e.g., optical motion tracking based prospective motion correction (Zaitsev et al., 2010), need to be combined with in future MRS studies.

In summary, compared to manual voxel prescription, automatic voxel prescription is demonstrated to prescribe MRS voxels with higher accuracy and reproducibility in a 7 T longitudinal MRS study. Therefore, the application of automatic instead of manual voxel prescription should be proposed in any future high field longitudinal MRS studies.

# 6

## Summary

## Summary

---

In this thesis, a comparison study is initially implemented to systematically compare the spectral separation between glutamine (Gln) and glutamate (Glu) at short echo time (TE) / mixing time (TM) and field-specific long TE/TM in stimulated-echo acquisition mode (STEAM) acquisition at 3 and 7 T. Short TE/TM (20 ms / 10 ms) at 7 T is proven to provide the spectra with highest signal-to-noise ratio (SNR) and thus better separate the *in vivo* Gln and Glu signals than long TE/TM (74 ms / 68 ms) proposed for best separation of main peaks of Gln and Glu (Yang et al., 2008). Based on this important finding, STEAM with short TE/TM (20 ms / 10 ms) is further applied at 7 T to systematically measure local Gln and Glu concentrations across the cingulate cortex (CC) of human brains. The reproducibility of Gln and Glu measurements is confirmed, and the regional variations of local Gln, Glu as well as GABA concentrations across the CC are revealed. In addition, automatic voxel prescription is applied for the first time to prescribe spectroscopy voxels in a 7 T longitudinal *in vivo* magnetic resonance spectroscopy (MRS) study. The accuracy and reproducibility of automatic voxel prescription is demonstrated to be much higher than manual voxel prescription.

The concentration levels of Gln and Glu are important indicators in neurological and psychiatric disease diagnosis. However, due to the severely overlapped spectra between the two, accurate estimation of Gln and Glu is so far largely limited. Previously proposed techniques, such as spectral editing and 2D-spectroscopy, for Gln and Glu acquisitions are not very suitable to be applied in clinical MRS studies, since the spectral editing techniques usually focus on only one metabolite while suppressing the other and 2D spectroscopy requires long acquisition time and large MRS voxels. In comparison, STEAM is reported to be capable of measuring metabolites efficiently and simultaneously within small voxels (Graaf and Rothman, 2001). As the lineshapes of Gln and Glu spectra in STEAM acquisition are strongly depended on the choice of TE and TM values (Thompson and Allen, 2001), this thesis initially investigates the optimal TE/TM setting in STEAM for Gln and Glu detection and demonstrates that short TE/TM (20 ms / 10 ms) can best separate *in vivo* Gln and Glu at 7 T. Based on the introduced accurate

## Summary

---

metabolite quantification by best spectral separation and further proved high reproducibility of Gln and Glu measurements, STEAM with short TE/TM (20 ms / 10 ms) at 7 T is proposed as a suitable method to measure Gln and Glu in clinical MRS studies. In addition, the measurements for those metabolites with small signals (e.g., GABA; Northoff et al., 2007), which are usually impossible to be detected at lower field, are also benefitted from the application of STEAM with TE/TM (20 ms / 10 ms) at 7 T, due to high spectral SNR provided by short TE at 7 T. Therefore, STEAM with short TE/TM (20 ms / 10 ms) can be further applied in future high field *in vivo* MRS studies.

In addition, the regional distributions of local Gln, Glu and GABA concentrations across the cingulate sub-regions are for the first time revealed in this thesis and compared to the profiles of respective local receptors proposed by Palomero-Gallagher et al., (2009). The GABA and Glu concentrations in the pregenual anterior CC (pgACC) region are higher compared to other sub-regions, while Gln concentrations are reversely increased in the rostro-caudal direction with the highest concentrations in the pgACC region. Furthermore, the concentration profiles of GABA and Glu are found to agree with the GABA<sub>B</sub> receptor fingerprints in the anterior CC, whereas the Gln patterns are consistent with AMPA receptor distributions. Considering that the varied gray matter (GM) contents across the CC can potentially influence the metabolite concentrations, one new concentration correction method for GM content is designed and applied to correct metabolite concentrations.

At last, due to the potential interference between voxel position detection and high field inhomogeneity, no automatic voxel prescription has been applied in high field longitudinal MRS studies so far. Manual voxel prescription, as the traditional method to localize spectroscopy voxels, can introduce variability of voxel positions between different scan sessions and also require additional scan time for careful voxel adjustments (e.g., localization and orientation) at multiple scan sessions. Both drawbacks are in many cases challenging in particular the longitudinal MRS studies.

## Summary

---

Therefore, in the last section of this thesis, a vendor-provided automatic voxel positioning technique is tested in a 7 T longitudinal *in vivo* MRS study. The achieved highly accurate and reproducible voxel prescription, plus the fast running time, indicates that automatic instead of manual voxel prescription should be applied in any future high field longitudinal *in vivo* MRS studies.

In conclusion, this thesis firstly proposes the application of STEAM with short TE/TM (20 ms / 10 ms) at 7 T for any upcoming *in vivo* Gln- and Glu-oriented MRS studies, and secondly demonstrates that the automatic instead of manual voxel prescription should be used in future high field longitudinal *in vivo* MRS studies.

# BIBLIOGRAPHY

- Albrecht J, Sidoryk-Węgrzynowicz M, Zielińska M, Aschner M (2010) Roles of glutamine in neurotransmission. *Neuron Glia Biol.* 6:263–276.
- Altamura C, Maes M, Dai J, Meltzer HY (1995) Plasma concentrations of excitatory amino acids, serine, glycine, taurine and histidine in major depression. *Eur Neuropsychopharmacol* 5:71–75.
- Ashburner J, Barnes G, Chen C, Daunizeau J, Flandin G, Friston K, Kiebel S, Kilner J, Litvak V, Moran R, Penny W, Rosa M, Stephan K, Gitelman D, Henson R, Hutton C, Glauche V, Mattout J, Phillips C (2013) SPM8 Manual. <http://www.fil.ion.ucl.ac.uk/spm/>. Accessed 4 February 2013.
- Balci M (2005) Basic  $^1\text{H}$ - and  $^{13}\text{C}$ -NMR spectroscopy. Amsterdam, Boston: Elsevier.
- Bartha R, Drost D, Menon R, Williamson P (2000) Comparison of the quantification precision of human short echo time  $^1\text{H}$  spectroscopy at 1.5 and 4.0 Tesla. *Magn. Reson. Med.* 44:185–192.
- Becker ED (2000) High resolution NMR. Theory and chemical applications. San Diego, CA: Academic Press.
- Benner T, Wisco JJ, van der Kouwe AJ, Fischl B, Vangel MG, Hochberg FH, Sorensen AG (2006) Comparison of manual and automatic section positioning of brain MR images. *Radiology* 239:246–254.
- Bernstein MA, King KF, Zhou XJ (2004) Handbook of MRI pulse sequences. Amsterdam, Boston: Academic Press.
- Bigler P (1997) NMR Spectroscopy: Processing Strategies. Weinheim, Germany: Wiley-VCH Verlag GmbH.
- Blümich B (2005) Essential NMR for scientists and engineers. Berlin: Springer.
- Brambilla P, Glahn DC, Balestrieri M, Soares JC (2005) Magnetic resonance findings in bipolar disorder. *Psychiatr. Clin. North Am.* 28:443–467.
- Breitmaier E, Voelter W (1987) Carbon-13 NMR Spectroscopy. Weinheim: Verlag Chemie.

## BIBLIOGRAPHY

---

- Brown MA, Semelka RC (2003) MRI. Basic principles and applications. Hoboken, N.J: Wiley-Liss.
- Cavassila S, Deval S, Huegen C, van Ormondt D, Graveron-Demilly D (2001) Cramér–Rao bounds: an evaluation tool for quantitation. *NMR Biomed.* 14:278–283.
- Chalifoux JR, Carter AG (2010) GABAB receptors modulate NMDA receptor calcium signals in dendritic spines. *Neuron* 66:101–113.
- Chen T, Zhan Y, Zhang S, Dewan M (2011) Automatic alignment of brain MR scout scans using data-adaptive multi-structural model. *Med. Image Comput. Comput. Assist. Interv.* 14:574–581.
- Clementi V, Tonon C, Lodi R, Malucelli E, Barbiroli B, Iotti S (2005) Assessment of glutamate and glutamine contribution to in vivo N-acetylaspartate quantification in human brain by (1)H-magnetic resonance spectroscopy. *Magn. Reson. Med.* 54:1333–1339.
- Conolly S, Glover G, Nishimura D, Macovski A (1991) A reduced power selective adiabatic spin-echo pulse sequence. *Magn. Reson. Med.* 18:28–38.
- Daikhin Y, Yudkoff M (2000) Compartmentation of brain glutamate metabolism in neurons and glia. *J. Nutr.* 130:1026S-31S.
- Dou W, Palomero-Gallagher N, van Tol M, Kaufmann J, Zhong K, Bernstein H, Heinze H, Speck O, Walter M (2013) Systematic regional variations of GABA, glutamine, and glutamate concentrations follow receptor fingerprints of human cingulate cortex. *J. Neurosci.* 33:12698–12704.
- Du J, Suzuki K, Wei Y, Wang Y, Blumenthal R, Chen Z, Falke C, Zarate CA, Manji HK (2006) The Anticonvulsants Lamotrigine, Riluzole, and Valproate Differentially Regulate AMPA Receptor Membrane Localization: Relationship to Clinical Effects in Mood Disorders. *Neuropsychopharmacology* 32:793–802.
- Elywa M, Mulla-Osman S, Godenschweger F, Speck O (2012) Proton magnetic resonance spectroscopy in deep human brain structures at 7 T. *J Appl Spectrosc* 79:120–125.
- Erecińska M, Silver IA (1990) Metabolism and role of glutamate in mammalian brain. *Prog. Neurobiol.* 35:245–296.

## BIBLIOGRAPHY

---

- Frahm J, Bruhn H, Gyngell ML, Merboldt KD, Hänicke W, Sauter R (1989) Localized proton NMR spectroscopy in different regions of the human brain in vivo. Relaxation times and concentrations of cerebral metabolites. *Magn. Reson. Med.* 11:47–63.
- Freeborough PA, Woods RP, Fox NC (1996) Accurate registration of serial 3D MR brain images and its application to visualizing change in neurodegenerative disorders. *J. Comput. Assist. Tomogr.* 20:1012–1022.
- Gedat E, Braun J, Sack I, Bernarding J (2004) Prospective registration of human head magnetic resonance images for reproducible slice positioning using localizer images. *J. Magn. Reson. Imaging* 20:581–587.
- Govindaraju V, Young K, Maudsley AA (2000) Proton NMR chemical shifts and coupling constants for brain metabolites. *NMR Biomed.* 13:129–153.
- Graaf RA de, Rothman DL (2001) In vivo detection and quantification of scalar coupled <sup>1</sup>H NMR resonances. *Concepts Magn. Reson.* 13:32–76.
- Hargreaves BA, Cunningham CH, Nishimura DG, Conolly SM (2004) Variable-rate selective excitation for rapid MRI sequences. *Magn. Reson. Med.* 52:590–597.
- Henry ME, Lauriat TL, Shanahan M, Renshaw PF, Jensen JE (2011) Accuracy and stability of measuring GABA, glutamate, and glutamine by proton magnetic resonance spectroscopy: A phantom study at 4Tesla. *J. Magn. Reson.* 208:210–218.
- Horn DI, Yu C, Steiner J, Buchmann J, Kaufmann J, Osoba A, Eckert U, Zierhut KC, Schiltz K, He H, Biswal B, Bogerts B, Walter M (2010) Glutamatergic and resting-state functional connectivity correlates of severity in major depression - the role of pregenual anterior cingulate cortex and anterior insula. *Front Syst. Neurosci.* 4:33.
- Houkin K, Kamada K, Kamiyama H, Iwasaki Y, Abe H, Kashiwaba T (1993) Longitudinal changes in proton magnetic resonance spectroscopy in cerebral infarction. *Stroke* 24:1316–1321.
- Hurd R, Sailasuta N, Srinivasan R, Vigneron DB, Pelletier D, Nelson SJ (2004) Measurement of brain glutamate using TE-averaged PRESS at 3T. *Magn. Reson. Med.* 51:435–440.

## BIBLIOGRAPHY

---

- Itti L, Chang L, Ernst T (2001) Automatic scan prescription for brain MRI. *Magn. Reson. Med.* 45:486–494.
- Jacobsen NE (2007) *Understanding nuclear magnetic resonance spectroscopy. A practical guide.* Hoboken, N.J, Chichester: Wiley; John Wiley.
- Kakeda S, Korogi Y, Moriya J, Ohnari N, Sato T, Ueno S, Yanagihara N, Harada M, Matsuda T (2011) Influence of work shift on glutamic acid and gamma-aminobutyric acid (GABA): Evaluation with proton magnetic resonance spectroscopy at 3T. *Psychiatry Res.* 192:55–9.
- Keeler J (2002) *Understanding NMR spectroscopy.* Chichester: Wiley.
- Klose U (1990) In vivo proton spectroscopy in presence of eddy currents. *Magn. Reson. Med.* 14:26–30.
- Kreis R, Ernst T, Ross B (1993) Absolute Quantitation of Water and Metabolites in the Human Brain. II. Metabolite Concentrations. *Journal of Magnetic Resonance, Series B* 102:9–19.
- Lee HK, Yaman A, Nalcioglu O (1995) Homonuclear J-refocused spectral editing technique for quantification of glutamine and glutamate by  $^1\text{H}$  NMR spectroscopy. *Magn. Reson. Med.* 34:253–259.
- Levine J, Panchalingam K, Rapoport A, Gershon S, McClure RJ, Pettegrew JW (2000) Increased cerebrospinal fluid glutamine levels in depressed patients. *Biol. Psychiatry* 47:586–593.
- Li Y, Xu D, Chen A, Vigneron D, Nelson S (2008) Proton spectroscopy of human brain at 3T and 7T: signal-to-noise ratio, spectral linewidth and relaxation times. *Proceedings of the Sixteenth Annual Meeting of International Society for Magnetic Resonance in Medicine, Toronto, Canada: ISMRM; 1592.*
- Lockhart ME, Fielding JR, Richter HE, Brubaker L, Salomon CG, Ye W, Hakim CM, Wai CY, Stolpen AH, Weber AM (2008) Reproducibility of Dynamic MR Imaging Pelvic Measurements: A Multi-institutional Study. *Radiology* 249:534–540.

## BIBLIOGRAPHY

---

- Lynch J, Peeling J, Auty A, Sutherland GR (1993) Nuclear magnetic resonance study of cerebrospinal fluid from patients with multiple sclerosis. *Can. J. Neurol. Sci.* 20:194–198.
- Mandal PK (2007) Magnetic resonance spectroscopy (MRS) and its application in Alzheimer's disease. *Concepts Magn. Reson.* 30:40–64.
- Mayer D, Spielman DM (2005) Detection of glutamate in the human brain at 3 T using optimized constant time point resolved spectroscopy. *Magn. Reson. Med.* 54:439–442.
- McLean MA, Woermann FG, Barker GJ, Duncan JS (2000) Quantitative analysis of short echo time (1)H-MRSI of cerebral gray and white matter. *Magn. Reson. Med.* 44:401–411.
- Moats RA, Ernst T, Shonk TK, Ross BD (1994) Abnormal cerebral metabolite concentrations in patients with probable Alzheimer disease. *Magn. Reson. Med.* 32:110–115.
- Molyneux PD, Tofts PS, Fletcher A, Gunn B, Robinson P, Gallagher H, Moseley IF, Barker GJ, Miller DH (1998) Precision and reliability for measurement of change in MRI lesion volume in multiple sclerosis: a comparison of two computer assisted techniques. *J. Neurol. Neurosurg. Psychiatry* 65:42–47.
- Northoff G, Walter M, Schulte RF, Beck J, Dydak U, Henning A, Boeker H, Grimm S, Boesiger P (2007) GABA concentrations in the human anterior cingulate cortex predict negative BOLD responses in fMRI. *Nat. Neurosci.* 10:1515–1517.
- Öz G, Tkáč I (2011) Short-echo, single-shot, full-intensity proton magnetic resonance spectroscopy for neurochemical profiling at 4 T: Validation in the cerebellum and brainstem. *Magn. Reson. Med.* 65:901–10.
- Palomero-Gallagher N, Vogt BA, Schleicher A, Mayberg HS, Zilles K (2009) Receptor architecture of human cingulate cortex: Evaluation of the four-region neurobiological model. *Hum. Brain Mapp.* 30:2336–2355.

## BIBLIOGRAPHY

---

- Pan JW, Mason GF, Pohost GM, Hetherington HP (1996) Spectroscopic imaging of human brain glutamate by water-suppressed J-refocused coherence transfer at 4.1 T. *Magn. Reson. Med.* 36:7–12.
- Petroff OA, Rothman DL, Behar KL, Lamoureux D, Mattson RH (1996) The effect of gabapentin on brain gamma-aminobutyric acid in patients with epilepsy. *Ann. Neurol.* 39:95–99.
- Pfleiderer B, Michael N, Erfurth A, Ohrmann P, Hohmann U, Wolgast M, Fiebich M, Arolt V, Heindel W (2003) Effective electroconvulsive therapy reverses glutamate/glutamine deficit in the left anterior cingulum of unipolar depressed patients. *Psychiatry Res.* 122:185-192.
- Provencher SW (1993) Estimation of metabolite concentrations from localized in vivo proton NMR spectra. *Magn. Reson. Med.* 30:672–679.
- Provencher SW (November 16th, 2013) LCMModel & LCMgui User's Manual. <http://s-provencher.com/pages/lcm-manual.shtml>.
- Salvadore G, van der Veen JW, Zhang Y, Marengo S, Machado-Vieira R, Baumann J, Ibrahim LA, Luckenbaugh DA, Shen J, Drevets WC, Zarate CA (2012) An investigation of amino-acid neurotransmitters as potential predictors of clinical improvement to ketamine in depression. *Int. J. Neuropsychopharmacol.* 15:1063–1072.
- Sanacora G, Mason GF, Rothman DL, Behar KL, Hyder F, Petroff OA, Berman RM, Charney DS, Krystal JH (1999) Reduced cortical gamma-aminobutyric acid levels in depressed patients determined by proton magnetic resonance spectroscopy. *Arch. Gen. Psychiatry* 56:1043–1047.
- Schott JM, Frost C, MacManus DG, Ibrahim F, Waldman AD, Fox NC (2010) Short echo time proton magnetic resonance spectroscopy in Alzheimer's disease: a longitudinal multiple time point study. *Brain* 133:3315–3322.
- Schubert F, Gallinat J, Seifert F, Rinneberg H (2004) Glutamate concentrations in human brain using single voxel proton magnetic resonance spectroscopy at 3 Tesla. *Neuroimage* 21:1762–1771.

## BIBLIOGRAPHY

---

- Schulte RF, Trabesinger AH, Boesiger P (2005) Chemical-shift-selective filter for the in vivo detection of J-coupled metabolites at 3T. *Magn. Reson. Med.* 53:275–281.
- Sharp GC, Kollipara S, Madden T, Jiang SB, Rosenthal SJ (2005) Anatomic feature-based registration for patient set-up in head and neck cancer radiotherapy. *Phys. Med. Biol.* 50:4667–4679.
- Smith S, Levante T, Meier B, Ernst R (1994) Computer Simulations in Magnetic Resonance. An Object-Oriented Programming Approach. *Journal of Magnetic Resonance, Series A* 106:75–105.
- Soher B, Semanchuk P, Young K, Todd D (January 30th, 2013) VeSPA - Simulation User Manual and Reference. <http://scion.duhs.duke.edu/vespa/simulation>.
- Srinivasan R, Cunningham C, Chen A, Vigneron D, Hurd R, Nelson S, Pelletier D (2006) TE-averaged two-dimensional proton spectroscopic imaging of glutamate at 3 T. *Neuroimage* 30:1171–1178.
- Stephenson MC, Gunner F, Napolitano A, Greenhaff PL, Macdonald IA, Saeed N, Vennart W, Francis ST, Morris PG (2011) Applications of multi-nuclear magnetic resonance spectroscopy at 7T. *World J. Radiol.* 3:105–113.
- Taylor-Robinson SD, Weeks RA, Bryant DJ, Sargentoni J, Marcus CD, Harding AE, Brooks DJ (1996) Proton magnetic resonance spectroscopy in Huntington's disease: evidence in favour of the glutamate excitotoxic theory. *Mov. Disord.* 11:167–173.
- Thomas MA, Ryner LN, Mehta MP, Turski PA, Sorenson JA (1996) Localized 2D J-resolved <sup>1</sup>H MR spectroscopy of human brain tumors in vivo. *J. Magn. Reson. Imaging* 6:453–459.
- Thompson RB, Allen PS (1998) A new multiple quantum filter design procedure for use on strongly coupled spin systems found in vivo: its application to glutamate. *Magn. Reson. Med.* 39:762–771.
- Thompson RB, Allen PS (2001) Response of metabolites with coupled spins to the STEAM sequence. *Magn. Reson. Med.* 45:955–965.
- Tkác I, Andersen P, Adriany G, Merkle H, Ugurbil K, Gruetter R (2001) In vivo <sup>1</sup>H NMR spectroscopy of the human brain at 7 T. *Magn. Reson. Med.* 46:451–456.

## BIBLIOGRAPHY

---

- Tkáč I, Öz G, Adriany G, Uğurbil K, Gruetter R (2009) In vivo  $^1\text{H}$  NMR spectroscopy of the human brain at high magnetic fields: Metabolite quantification at 4T vs. 7T. *Magn. Reson. Med.* 62:868–879.
- van de Moortele P, Auerbach EJ, Olman C, Yacoub E, Uğurbil K, Moeller S (2009) T1 weighted brain images at 7 Tesla unbiased for Proton Density,  $T_2^*$  contrast and RF coil receive B1 sensitivity with simultaneous vessel visualization. *Neuroimage* 46:432–446.
- van der Kouwe AJ, Benner T, Fischl B, Schmitt F, Salat DH, Harder M, Sorensen AG, Dale AM (2005) On-line automatic slice positioning for brain MR imaging. *NeuroImage* 27:222–230.
- Walter M, Henning A, Grimm S, Schulte RF, Beck J, Dydak U, Schnepf B, Boeker H, Boesiger P, Northoff G (2009) The relationship between aberrant neuronal activation in the pregenual anterior cingulate, altered glutamatergic metabolism, and anhedonia in major depression. *Arch. Gen. Psychiatry* 66:478–486.
- Weir JP (2005) Quantifying test-retest reliability using the intraclass correlation coefficient and the SEM. *J. Strength Cond. Res.* 19:231–240.
- Welch EB, Manduca A, Grimm RC, Ward HA, Jack CR Jr (2002) Spherical navigator echoes for full 3D rigid body motion measurement in MRI. *Magn. Reson. Med.* 47:32–41.
- Welch EB, Manduca A, Grimm RC, Jack CR Jr (2004) Interscan registration using navigator echoes. *Magn. Reson. Med.* 52:1448–1452.
- Yang S, Hu J, Kou Z, Yang Y (2008) Spectral simplification for resolved glutamate and glutamine measurement using a standard STEAM sequence with optimized timing parameters at 3, 4, 4.7, 7, and 9.4T. *Magn. Reson. Med.* 59:236–244.
- Yildiz-Yesiloglu A, Ankerst DP (2006) Review of  $^1\text{H}$  magnetic resonance spectroscopy findings in major depressive disorder: a meta-analysis. *Psychiatry Res.* 147:1–25.
- Yu C, Zhou Y, Liu Y, Jiang T, Dong H, Zhang Y, Walter M (2011) Functional segregation of the human cingulate cortex is confirmed by functional connectivity based neuroanatomical parcellation. *NeuroImage* 54:2571–2581.

## BIBLIOGRAPHY

---

Zaitsev M, Speck O, Hennig J, Büchert M (2010) Single-voxel MRS with prospective motion correction and retrospective frequency correction. *NMR Biomed.* 23(3):325-332.

Zhang L, Xu Q, Chen C, Novak CL (2009) Automated alignment of MRI brain scan by anatomic landmarks. *SPIE. Med. Imag.* vol.:7258.

## OWN PUBLICATIONS

### Journal Articles

1. **Dou W**, Palomero-Gallagher N, van Tol MJ, Kaufmann J, Zhong K, Bernstein HG, Heinze HJ, Speck O, Walter M (2013) Systematic regional variations of GABA, glutamine, and glutamate concentrations follow receptor fingerprints of human cingulate cortex. *J. Neurosci.* 33:12698–12704.
2. **Dou W**, Speck O, Benner T, Kaufmann J, Li M, Zhong K, Walter M (2014) Automatic voxel positioning for MRS at 7 T. *Magn Reson Mater Phy*, DOI: 10.1007/s10334-014-0469-9 (E-pub).
3. Li M, Metzger CD, Li W, Safron A, van Tol MJ, Lord A, Krause AL, Borchardt V, **Dou W**, Genz A, Heinze HJ, He H, Walter M (2014) Dissociation of glutamate and cortical thickness is restricted to regions subserving trait but not state markers in major depressive disorder. *J. Affect Disord.* 169:91–100.

### International Conferences

1. K Zhong, R Deichmann, **W Dou** and O Speck (2010)  $T_2^*$  mapping at 7T. Joint Annual Meeting ISMRM-ESMRMB 2010, Stockholm, Sweden. (Poster)
2. **W Dou**, R Deichmann, O Speck and K Zhong (2011) Improving  $T_2^*$  mapping at 7T. 19<sup>th</sup> scientific meeting of ISMRM, Montréal, Canada. (Poster)
3. **W Dou**, R Yakupov, J Kaufmann, M van Tol, C Yang, O Speck and M Walter (2012) Retest reliability and systematic regional variations of Glu, Gln and GABA concentrations using STEAM with VERSE in a longitudinal multi-voxel study at 7 Tesla. 29<sup>th</sup> scientific meeting of ESMRMB, Lisbon, Portugal. (Oral)

## OWN PUBLICATIONS

---

4. **W Dou**, J Kaufmann, M Walter, and O Speck (2013) What is the best TE/TM in STEAM to resolve Gln/Glu at 7T? 30<sup>th</sup> scientific meeting of ESMRMB, Toulouse, France. (E-Poster).
5. M Walter, **W Dou**, J Kaufmann, M van Tol and O Speck (2013) Neurotransmitter balance follows GABA receptor profiles in cingulate cortex - A multivoxel MRS study. 19<sup>th</sup> annual meeting of the organization for Human Brain Mapping, Seattle, USA. (Poster).
6. **W Dou**, J Kaufmann, M Li, M Walter, and O Speck (2014) Validation of automatic voxel positioning for MRS at 7T. Joint Annual Meeting ISMRM-ESMRMB 2014, Milan, Italy. (E-Poster).

## ACKNOWLEDGEMENTS

---

# ACKNOWLEDGEMENTS

I wish to express my thanks to many persons helping and inspiring me during my doctoral studies.

I especially wish to express my sincere appreciation to my first supervisor, Prof. Dr. Oliver Speck, head of the Department of Biomedical Magnetic Resonance (BMMR), Otto-von-Guericke University of Magdeburg, for his excellent guidance, caring, patience, friendship, and wisdom. He provided me with an excellent atmosphere, encouragement, inspiration, and motivation for doing research and enabled me to complete my doctoral studies smoothly and successfully.

I would also wish to express my deep appreciation to my second supervisor PD. Dr. Martin Walter, head of the Department of Clinical Affective Neuroimaging Laboratory (CANLAB), Leibniz Institute for Neurobiology & Otto-von-Guericke University of Magdeburg. Without his brilliant guidance, patience and financial support, I could not finish the research work on time.

Additionally, special thanks to Dr. Martin Kanowski and Dr. Jörn Kaufmann for their professional advices and generous helps. Discussions with them about my work were very helpful for this study.

Thanks also to our BMMR group members (Dr. Myung-Ho In, Dr. Niravkumar K. Darji, Dr. Shang Yang, Dipl. Tobias Leutritz and Dr. Frank Godenschweger) for their valuable helps and suggestions in research and life through our interactions during the long hours in the office.

I am very grateful to my parents, my grandparents and my uncles. They were always supporting and encouraging me with their best wishes.

Last but not least, I am greatly indebted to my devoted wife Sally (Pingping). Her love and support without any complaints have allowed me complete this doctoral study.

Magdeburg, Germany

Weiqliang Dou

June 2014

## ERKLÄRUNG

Hiermit erkläre ich, dass ich die von mir eingereichte Dissertation zum dem Thema

**“The Investigation of Glutamine and Glutamate in the Human Brain Using MR Spectroscopy at 7 Tesla”**

selbständig verfasst, nicht schon als Dissertation verwendet habe und die benutzten Hilfsmittel und Quellen vollständig angegeben wurden.

Weiterhin erkläre ich, dass ich weder diese noch eine andere Arbeit zur Erlangung des akademischen Grades doctor rerum naturalium (Dr. rer. nat.) an einer anderen Einrichtungen eingereicht habe.

Magdeburg,

June 2014

Weiqiang Dou

## LEBENS LAUF

---

<b>Geburtstag</b>	25. Mai 1985 in Nanjing, China
<b>Nationalität</b>	China
<b>Familienstand</b>	verheiratet
<b>Adresse</b>	J.-G.-Nathusius- Ring 5, Zi.Nr.425, 39106, Magdeburg
<b>Telefon</b>	0391/6117123
<b>E-Mail</b>	weiqiang.dou@ovgu.de

### Ausbildung

---

<b>10/2010 bis heute</b>	<b>Promotionsstudent (PhD) in Physik</b> <i>Otto-von-Guericke-Universität Magdeburg</i> <i>Thema: "The Investigation of Glutamine and Glutamate in the Human Brain Using MR Spectroscopy at 7 Tesla "</i>
<b>4/2008 bis 8/2010</b>	<b>Master of Science (M.Sc.) (Abschlussnote: 1.8)</b> <i>Otto-von-Guericke-Universität Magdeburg</i>
<b>9/2003 bis 6/2007</b>	<b>Bachelor of Engineering (B.E.) (Abschlussnote: 2.3)</b> <i>Nanjing Institute of Technology</i>

### Ehrungen/Auszeichnungen

---

<b>5/2011</b>	<i>Ausbildungsstipendium für Studenten, Postdoktoranden und Klinische Auszubildende bei der ISMRM 2011 in Montréal, Kanada</i>
<b>5/2014</b>	<i>Ausbildungsstipendium für Studenten, Postdoktoranden und Klinische Auszubildende bei der ISMRM 2014 in Milano, Italian</i>